Theses and Dissertations   1. Thesis and Dissertation Collection, all items

1981-06

Acoustic boundary wave generation and shadowing at a seamount.

Jordan, Edgar Alvin

Monterey, California. Naval Postgraduate School

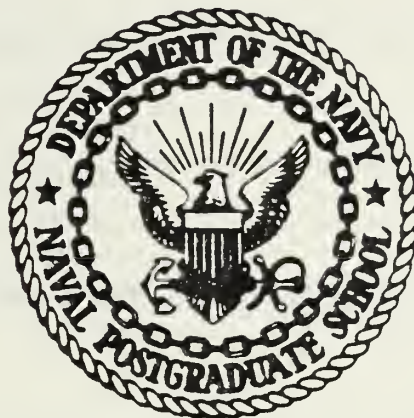http://hdl.handle.net/10945/20404

ACOUSTIC BOUNDARY WAVE GENERATION
AND SHADOWING AT A SEAMOUNT

Edgar Alvin Jordan

NAVAL POSTGRADUATE SCHOOL
Monterey, California

THESIS

ACOUSTIC BOUNDARY WAVE GENERATION AND
SHADOWING AT A SEAMOUNT

by

Edgar Alvin Jordan

June 1981

Thesis Advisor: H. Medwin

T200050

REPORT DOCUMENTATION PAGE		READ INSTRUCTIONS BEFORE COMPLETING FORM
1. REPORT NUMBER	2. GOVT ACCESSION NO.	3. RECIPIENT'S CATALOG NUMBER
4. TITLE (and Subtitle) Acoustic Boundary Wave Generation and Shadowing at a Seamount		5. TYPE OF REPORT & PERIOD COVERED Master's thesis; June 1981
		6. PERFORMING ORG. REPORT NUMBER
7. AUTHOR(s) Edgar Alvin Jordan		8. CONTRACT OR GRANT NUMBER(s)
9. PERFORMING ORGANIZATION NAME AND ADDRESS Naval Postgraduate School Monterey, California 93940		10. PROGRAM ELEMENT, PROJECT, TASK AREA & WORK UNIT NUMBERS
11. CONTROLLING OFFICE NAME AND ADDRESS Naval Postgraduate School Monterey, California 93940		12. REPORT DATE June 1981
		13. NUMBER OF PAGES 96
14. MONITORING AGENCY NAME & ADDRESS(If different from Controlling Office)		15. SECURITY CLASS. (of this report) Unclassified
		15a. DECLASSIFICATION/DOWNGRADING SCHEDULE

16. DISTRIBUTION STATEMENT (of this Report)

Approved for public release; distribution unlimited.

17. DISTRIBUTION STATEMENT (of the abstract entered in Block 20, if different from Report)

18. SUPPLEMENTARY NOTES

19. KEY WORDS (Continue on reverse side if necessary and identify by block number)

Boundary Wave
Topographical Shadowing
Diffraction
Forward Scattering
Random Roughness

20. ABSTRACT (Continue on reverse side if necessary and identify by block number)

The interaction of a sound field and a seamount has been studied by physically modeling the ocean surface over 2 dimensional and 3 dimensional models of Dickens Seamount. By using a smooth ocean surface, and one with a surface of scaled Rayleigh roughness to model a 35 knot wind, the relative contributions are determined for off-axis scattering elements, multiple reflection from the ocean surface, and diffraction over the crest of the seamount.

DD $_{1\ JAN\ 73}^{FORM}$ 1473   EDITION OF 1 NOV 65 IS OBSOLETE
(Page 1)   S/N 0102-014-6601 |

#20 - ABSTRACT - (CONTINUED)

Boundary wave generation over a randomly rough plane surface is studied experimentally. The ratio of boundary wave amplitude to volume wave amplitude is found to be proportional to (frequency)$^{3/2}$ and (range)$^{1/2}$ and the ratio of the empirical scattering parameter to the rms height of the roughness elements is found to be approximately 0.3. The spatial correlation length of the randomly rough surface takes the place of the center-to-center separation of the hemispherical bosses used in Tolstoy's theoretical treatment.

Acoustic Boundary Wave Generation and
Shadowing at a Seamount

by

Edgar Alvin Jordan
Lieutenant, United States Navy
B.S. Physics, Weber State College, 1974

Submitted in partial fulfillment of the
requirements for the degree of

MASTER OF SCIENCE IN ENGINEERING ACOUSTICS

from the

NAVAL POSTGRADUATE SCHOOL
June 1981

ABSTRACT

The interaction of a sound field and a seamount has been studied by physically modeling the ocean surface over 2 dimensional and 3 dimensional models of Dickens Seamount. By using a smooth ocean surface, and one with a surface of scaled Rayleigh roughness to model a 35 knot wind, the relative contributions are determined for off-axis scattering elements, multiple reflection from the ocean surface, and diffraction over the crest of the seamount.

Boundary wave generation over a randomly rough plane surface is studied experimentally. The ratio of boundary wave amplitude to volume wave amplitude is found to be proportional to $(frequency)^{3/2}$ and $(range)^{1/2}$ and the ratio of the empirical scattering parameter to the rms height of the roughness elements is found to be approximately 0.3. The spatial correlation length of the randomly rough surface takes the place of the center-to-center separation of the hemispherical bosses used in Tolstoy's theoretical treatment.

4

TABLE OF CONTENTS

LIST OF FIGURES

LIST OF TABLES

ACKNOWLEDGMENTS

I. INTRODUCTION

In previous work the interaction effect of an acoustic wave with an underwater barrier such as a seamount has been considered in terms of forward scatter at the upslope and diffraction over the crest. This work was grounded on the theoretical developments of Biot and Tolstoy [Ref. 1] which provided a solution to the problem of sound energy diffracted by a rigid, infinite wedge. Bremhorst [Ref. 2] was able to demonstrate close agreement between the Biot-Tolstoy theory and experimental measurements for a 90 degree wedge used as a diffracting barrier.

Spaulding [Ref. 3] extended this approach to a physical scale model of Dickens Seamount located in the Gulf of Alaska. In order to validate the laboratory model, Spaulding used the ocean data of Ebbeson et al., [Ref. 4] of the Canadian Defense Research Establishment, Pacific (DREP). Figure 1 supplied by DREP shows their 1978 ray patterns for three cases of inter-action of the sound field with Dickens Seamount. Spaulding addressed only case A where the rays appear to be completely blocked. Figure 2 shows that for case A there was a dis-crepancy of about 15 dB between theory and what was observed at sea. Concurrently, Medwin and Spaulding [Ref. 5] were able to extend the Biot-Tolstoy theory, show how it could be used for a finite wedge, and define the Diffraction Strength of a wedge-like crest as shown in Figure 3. However, in the
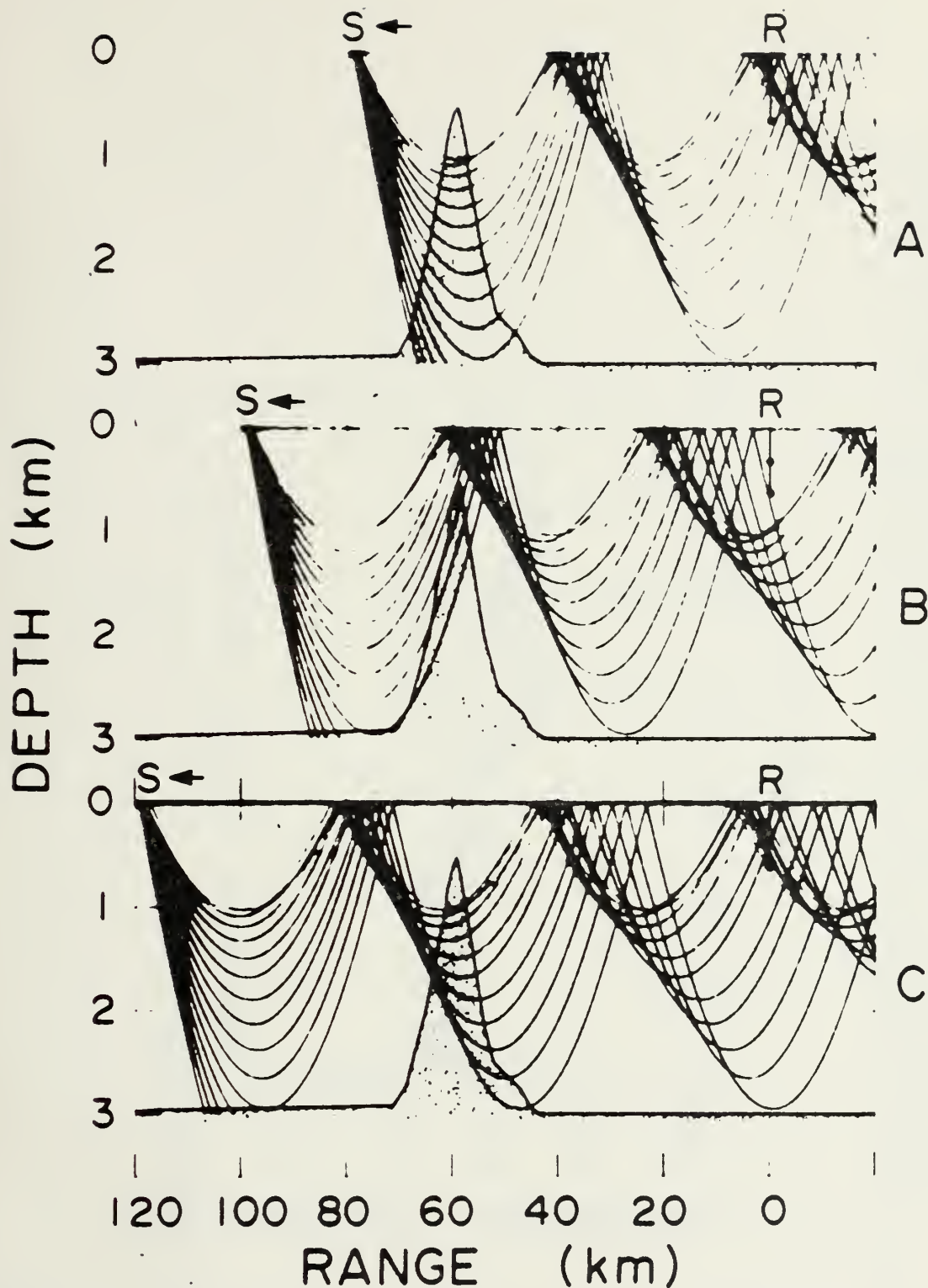
FIGURE 1. Ray traces for track 6. Source ranges are 79 Km (A), 99 Km (B), and 119 Km (C). Source depth = 18 m, receiver depths = 329 m, 633 m. The source angles are ±15° in 1° increments (from Ref. 4)
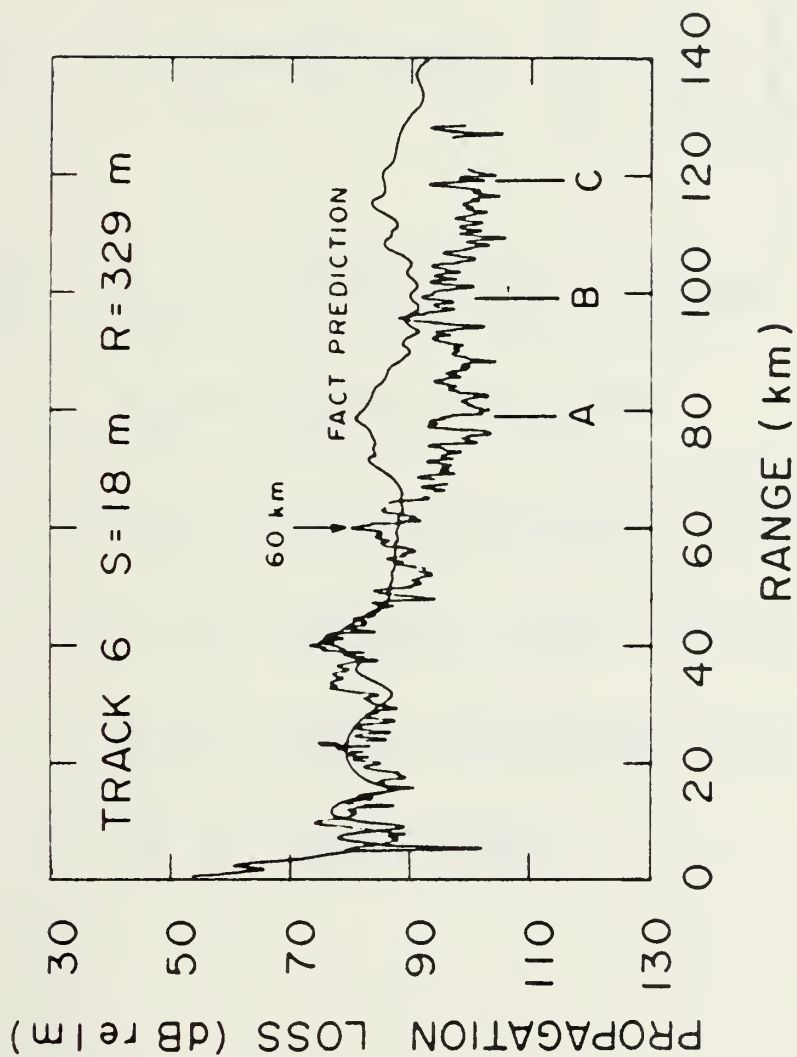
FIGURE 2.   Measured propagation loss for track 6 with the source at 18 m and receiver at 329 m. The smooth line is the FACT prediction based on a flat bottom. The arrow indicates the seamount range (from Ref. 4)

12

$$DS(\theta,\ \theta_0,\ r,\ r_0) = 20\ \text{Log}_{10}\ \frac{P_d}{P_0}\ \frac{r_0}{R_0}\ \sqrt{\frac{r}{\lambda}}$$

WHERE P_d =   DIFFRACTED PRESSURE

             P_0 =   SOURCE PRESSURE

             r_0 =   DISTANCE SOURCE TO CREST

             r =   DISTANCE CREST TO RECEIVER

             R_0 =   SOURCE REFERENCE DISTANCE

             λ =   WAVE LENGTH

FIGURE 3.   Diffraction strength, Definition (from Ref. 5)

work, Spaulding did not consider the effects of the inter-
action of the sound energy with the ocean surface above it.

In May 1978 Tolstoy [Ref. 6] presented a new theory of
acoustic scatter from a slightly rough surface at near graz-
ing incidence which incorporated the boundary condition for
a rough surface developed by Biot [Ref. 7]. This theory
represented a significant departure from more traditional
approaches to the problem of acoustic scatter for three pri-
mary reasons: First, the theory is first order in the rough-
ness parameter, as opposed to more conventional approaches
which consider the roughness parameter a second order effect:
Second, the theory includes multiple scatter and diffraction
which is generally ignored by other theories: Third, Tolstoy's
theory does not make the Kirchhoff Assumption which is par-
ticularly untenable at low grazing angles.

The surprising result of Tolstoy's theory is the predic-
tion of the existence of what he called a "boundary wave" in
the fluid above a slightly rough surface generated at near-
grazing incidence by coherent multiple Rayleigh scatter.
Since the $r^{1/2}$ power law Tolstoy derived for the range de-
pendence of the ratio of the boundary wave to the volume
wave (the volume wave is that wave which exists in the fluid
well above the scattering surface) was that of cylindrical
spreading instead of the spherical spreading which the volume
wave suffers; the theory also predicted that as the range
increased, the boundary wave would become stronger than the

14

volume wave at some range. This effect was first observed by Bailie [Ref. 8] for the case of scattering by closely packed hemispherical bosses on a rigid planar surface. The agreement between Bailie's results and Tolstoy's theory was quite remarkable.

The next author to consider the problem was Hollis [Ref. 9]. He addressed himself to a combination of the wedge problem and the coherent scatter problem by applying the hemispherical bosses used by Bailie to a 14 degree rigid wedge. The slope of 14 degrees was chosen because that corresponds to the average slope of Dickens Seamount. Hollis' results closely matched those of Bailie and again verified the predictions of Tolstoy by demonstrating the existence of the boundary wave. His results also showed for the highly idealized case of the 14 degree wedge roughened by hemispherical bosses, that the energy contained in the boundary wave as it diffracted over the crest of the wedge could be larger than the diffraction of the volume wave.

The purpose of this work is to consider the effects of including an appropriately roughened ocean surface above the model of Dickens Seamount for the geometry used by Spaulding and to investigate the possibility of extending Tolstoy's boundary wave theory to a randomly rough seamount surface.

II. <u>THEORY</u>

A. DIFFRACTION OVER A WEDGE

In general, diffraction occurs whenever an acoustic wave-
front encounters an obstacle of any sort. Of course, whether
the diffraction effects are important or if the phenomenon
being observed can be adequately represented by the approxi-
mations provided in ray theory, is a function of the specifics
of the problem under study. For the case of a source and
receiver separated by an infinite, rigid wedge with no direct
path between the two, diffraction provides the only mechanism
by which acoustic energy emanating from the source can reach
the receiver.

Consider the case of an infinite wedge represented in
Figure 4. The wedge is made up of two perfectly rigid plates,
which intersect at a crestline. This crest will provide a
convenient geometrical orientation and is thus designated as
the z axis of a cylindrical coordinate system. The region
in space not occupied by the wedge is filled with a homoge-
neous, compressible fluid of density ρ where sound travels
with velocity C. In such a system the displacement potential,
ϕ, is described by

$$\frac{\partial^2 \phi}{\partial r^2} + \frac{1}{r}\frac{\partial \phi}{\partial r} + \frac{1}{r^2}\frac{\partial^2 \phi}{\partial \theta^2} + \frac{\partial^2 \phi}{\partial z^2} = \frac{1}{C^2}\frac{\partial^2 \phi}{\partial t^2} \tag{1}$$

Harmonic solutions of this equation have the form
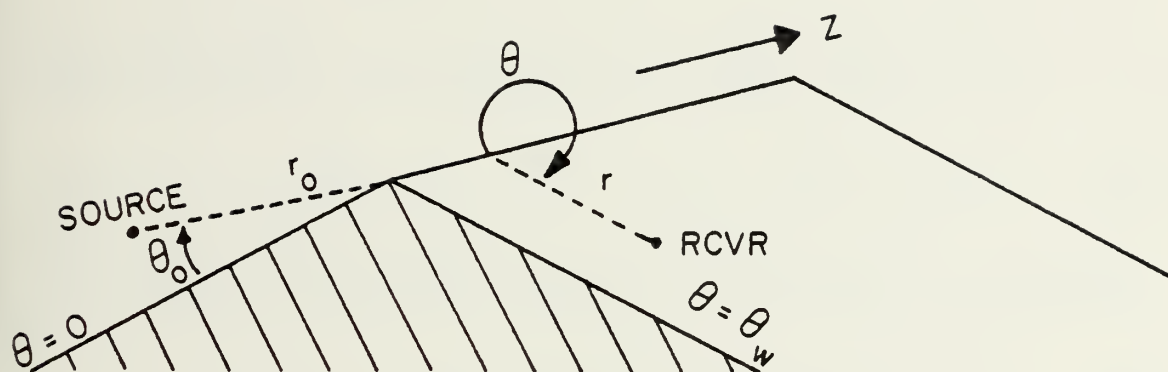
FIGURE 4. Geometry of Biot-Tolstoy theory for diffraction by a wedge. Wedge angle θ_w is measured in the fluid (from Ref. 5)

$$\phi = e^{\pm \nu \theta} H_{\nu}^{(1,2)}(kr) e^{\pm i \gamma z} e^{\pm \omega t} \qquad (2)$$

where

$$\gamma = \frac{\omega^2}{c^2} - k^2 \qquad (3)$$

and

$H_{\nu}^{(1,2)}$ are Bessels functions of the first kind

The rigid plates that make up the wedge require

$$\frac{\partial \phi}{\partial \theta} = 0 \quad \text{at} \quad \theta = 0 \quad \text{and} \quad \theta = \theta_w \qquad (4)$$

Applying this boundary condition to Equation (2) implies

$$\phi = \cos \nu_n \theta H_{\nu}^{(1,2)} e^{\pm i \gamma z} e^{\pm i \omega t} \qquad (5)$$

where

$$\nu_n = \frac{n \pi}{\theta_w}, \quad n = 0,1,2,\ldots \qquad (6)$$

Since at $r = 0$ the imaginary part of the Hankel function is infinite, it is further required that only the real part of $H_{\nu}^{(1,2)}$ will be retained.

Now assume a point source S (volume/time) which starts to flow uniformly and instantaneously at $t = 0$, so that at range R after time t

$$\frac{\partial \phi}{\partial t} = (-S/4 \pi R) \; 1 \; (t - R/C) \qquad (7)$$

Equation (5) is symmetric about the z axis. The normal coordinate method of Biot-Tolstoy is followed (see Ref. 1 for a detailed derivation of the method). Thus, the solution to Equation (1) becomes

$$\frac{\partial^2 \phi}{\partial t^2} = -\frac{C}{\partial_w} \sum_n \cos \nu_n \theta \cos \nu_n \theta_0 I_n \qquad (8)$$

for $ct \geq z$, where

$$I_n = \int_0^\infty J_{\nu_n}(kr) \, J_{\nu_n}(kr_0) \, J_0[k(c^2 t^2 - z^2)^{1/2}] k \; dk \qquad (9)$$

Using the transform detailed in Ref. 1, Equation (8) reduces to a form that is more easily visualized. Let

$$t_0 = \frac{1}{C}[(r - r_0)^2 + z^2]^{1/2}$$

$$\tau_0 = \frac{1}{C}[(r + r_0)^2 + z^2]^{1/2} \qquad (10)$$

t_0 is the time of travel of a pulse of sound from source to receiver by direct path. τ_0 is the time of travel from the source to the wedge crest then to the receiver. Thus, τ_0 is the time of travel of diffracted energy. This separates time, and therefore Equation (8), into three distinct regimes:

$$t < t_0$$

$$t_0 < t < \tau_0$$

$$\tau_0 < t$$

Since it is diffracted energy being considered, this implies solutions must be valid for $\tau_0 < t$. For this case

$$I_n = \frac{-1}{\pi r r_0 \sinh y} \sin \nu_n e^{-\nu_n y} \tag{11}$$

where

$$y = \cosh^{-1}\left[\frac{c^2 t^2 - (r^2 + r_0^2 + z^2)}{2 r r_0}\right] \tag{12}$$

Substituting the value for I_n back into Equation (8)

$$\frac{\partial^2 \phi}{\partial t^2} = \frac{C}{\pi \theta_w} \frac{1}{r r_0 \sinh y} \sum_n \cos \nu_n \theta_0 \cos \nu_n \theta \sin \nu_n \pi e^{-\nu_n y} \tag{13}$$

where $\tau_0 < t$ and y is given by Equation (12). Expressing the trigonometric functions as exponentials

$$\frac{\partial^2 \phi}{\partial t^2} = \frac{C}{4 \pi \theta_w} \frac{\exp(-\pi y/\theta_w)}{r r_0 \sinh y} \left[\frac{\sin(\pi/\theta_w)(\pi \pm \theta \pm \theta_0)}{1 - 2\exp(-\pi y/\theta_w)\cos(\pi/\theta_w)} \\ \cdot (\pi \pm \theta \pm \theta_0) + \exp(2\pi y/\theta_w)\right] \tag{14}$$

Since the acoustic pressure, p, and the displacement potential, ϕ, are related by

$$p = -\rho \frac{\partial^2 \phi}{\partial t^2} \tag{15}$$

The acoustic pressure due to the diffracted wave in the shadow zone of the wedge is

20

$$p = \frac{-\rho C}{4\pi\theta_w} \frac{\exp(-\pi y/\theta_w)}{r\, r_0 \sinh y}$$

$$\cdot \left[\frac{\sin(\pi/\theta_w)(\pi\pm\theta\pm\theta_0)}{1-2\exp(-\pi y/\theta_w)\cos(\pi/\theta_w)(\pi\pm\theta\pm\theta_0)+\exp(-2\pi y/\theta_w)} \right]$$

$$(16)$$

where

$$y = \cosh^{-1}\left[\frac{C^2 t^2 - (r^2 + r_0^2 + z^2)}{2\, r\, r_0} \right] \qquad (17)$$

and

θ_w = fluid region above the wedge

θ_0 = angle between wedge and source

θ = angle between wedge and receiver measured from source side of the wedge in the fluid above the wedge

r = distance from source to crest of the wedge

z = distance along the crest of the wedge where $z = 0$ represents the least time path from source to crest to receiver.

As pointed out by Spaulding [Ref. 10] the diffraction phenomenon can be described qualitatively as follows: The acoustic wave produced by a point source at a distance r from the crest of the wedge expands spherically. The wavefront first encounters the wedge crest at the point of least time travel path at time $t = r/C$ and $z = 0$. The wave will then continue to interact with the crest of the wedge at increasingly later time and increasing $|z|$. In effect, the crest of the

wedge acts as a continuous, time shaded, line source. Medwin
[Ref. 11] has computed the frequency transform of Equation
(16). It was this transform that Spaulding used to calcu-
late theoretical values to be compared with experimental
data for three models of Dickens Seamount of increasing
complexity.

B. BOUNDARY WAVE

I. Tolstoy has presented an application of a theory
developed by M. A. Biot [Ref. 12] formulating sound scatter from
slightly rough surfaces at near-grazing incidence. Tolstoy's
theory [Ref. 6] yields solutions for the coherent scatter of
transient spherical waves by rough planes where the size of
the roughness is small compared to the wave length of the
signal. Biot had previously demonstrated that if the spacing
between hemispherical bosses was small compared to a wave
length, they could be replaced with continuous distributions
of monopole and dipole radiators [Ref. 13].

To extend this formulation, Tolstoy assumed:

$$\frac{d}{\lambda} < \frac{h}{\lambda} << 1 \tag{18}$$

where

   d = diameter of hemispherical boss

   h = center to center spacing of bosses

   λ = acoustic wavelength

22

By applying the boundary condition formulated by Biot [Ref. 14], Tolstoy was able to show that for near-grazing incidence a boundary wave would be developed and that this boundary wave would decrease exponentially as the receiver was moved away from the plane of the hemispherical bosses. The temporal solution describing the pressure of the boundary was then transformed to the frequency domain using Fourier Transform techniques giving the pressure in the boundary wave as a function of frequency. The details of this development are contained in Ref. 6.

Thus, Tolstoy reported in 1979 that the amplitude of the postulated boundary wave as a function of frequency is

$$P_{BWA} = \frac{\varepsilon}{2C^2}[J_0^2(kr) + Y^2(kr)]^{1/2}\omega^2\exp[-\varepsilon(z+z_0)k^2] \quad (19)$$

where

ε = scattering parameter and is proportional to the volume of scatters per unit area

k = wave number

z = height of receiver above the plane

z_0 = height of source above the plane.

For the far field case where $kr \gg 1$, the entire scattered field can be written as

$$P_s(f) = \frac{\varepsilon}{2\pi} k^2\{\theta^2 + \frac{2\pi}{kr}\exp[-2\varepsilon k^2(z+z_0)]$$

$$+ 2(\frac{2\pi}{kr})^{1/2}\theta\sin(kr-\frac{\pi}{4})\exp[-\varepsilon k^2(z+z_0)]\}^{1/2} \quad (20)$$

23

where, for closely packed hemispherical bosses with center
to center distance, h, of 2 mm in air,

$$\varepsilon \;=\; 8.88 \times 10^{-5} \; m$$

$$k \;=\; \frac{2\pi f}{345} \; m^{-1}$$

r = range from source to receiver in meters

f = frequency in Hertz

z_0 = height of source in meters

z = height of receiver in meters

$$\theta \;=\; \arctan\left(\frac{z + z_0}{r}\right)$$

For the case of the source and receiver in the plane of the
roughness then, $z = z_0 = 0$ and Equations (19) and (20) reduce
to

$$P_s(f) \;=\; P_{BWA}(f) \;=\; \frac{\varepsilon}{2\pi} k^2 \left[\frac{2\pi}{kr}\right]^{1/2}$$

$$=\; \frac{\varepsilon \, k^{3/2}}{\sqrt{2\pi r}} \tag{21}$$

If the source is an impulse, then the acoustic pressure
generated by that source is

$$P_\delta \;=\; \frac{1}{2\pi r} \, \delta(t - r/C) \tag{22}$$

Transforming to the frequency domain

$$P_{VWA}(f) \;=\; \frac{1}{2\pi r} \tag{23}$$

24

If Equation (21) is divided by Equation (23), an expression
of the ratio of the boundary wave to the volume wave (spher-
ically spreading wave) is found which represents the frac-
tional change in wave amplitude in the plane of the hemispherical
bosses caused by those bosses

$$\frac{P_{BWA}}{P_{VWA}} = \varepsilon(2\pi r)^{1/2} k^{3/2} \tag{24}$$

It is this expression that was compared against experimental
data by Bailie [Ref. 15], Medwin, et al., [Ref. 16], and
Hollis [Ref. 17] and found to be in excellent agreement for
$kh \leq 1$.

III. RESEARCH FACILITIES AND EQUIPMENT

A. OCEAN PHYSICS LABORATORY AND ANECHOIC CHAMBER

The portion of the investigation dealing with the scale model of the Dickens Seamount was conducted in the Ocean Physics Laboratory located at the Naval Postgraduate School. The excellent signal to noise ratio provided by the source/ receiver selection made it unnecessary to use extraordinary quieting procedures, other than a relatively large number of signal averages prior to signal processing. The signal to noise ratio for this part of the experiment was never less than 20 dB from 20 kHz to 100 kHz for all of the work done in the laboratory itself. This fact allowed the investigation to proceed without requiring the seamount model to be moved. As the model is quite bulky and massive, this alone greatly facilitated the procedure.

On the other hand, that portion of the investigation dealing with forward scatter from a randomly rough plane surface was conducted in the Anechoic Chamber located next to the Ocean Physics Laboratory. This was a result of several factors all dictating a change in the source selection and the resultant decrease in available signal strength. As reported by Hollis [Ref. 18] receiver 4132 (with no source) in the Anechoic Chamber compared to the same receiver blocked by two sheets of 1/4 inch aluminum showed noise level differences of 0.1 dB or less over a frequency range of 2-30 kHz,

suggesting that the noise was electronic rather than acoustic.

B. DATA ACQUISITION AND PROCESSING EQUIPMENT

Data acquisition and processing was accomplished for both portions of the investigation by a digital computer system composed of four major components which were interfaced to provide high speed analog to digital conversion, data processing, data storage and output. The design, itself, was developed by the Special Projects Section, Naval Air Development Center in cooperation with Pinkerton Computer Consultants, Inc. of Warminster, Pennsylvania. The primary components of this system are as follows.

1. Interdata Model 70 Computer

This minicomputer has a 64 thousand byte core memory and is programmable in FORTRAN or BASIC. In addition to core memory, information can be stored on floppy disk or cassette tape for later processing.

2. Phoenix Analog to Digital Converter, Model ADC 712

The Model ADC 712, is a high speed, high accuracy analog voltage to digital converter which can encode a 20 volt, peak to peak, input signal into 12 binary bits, with a resultant resolution of one part in 4,095 at a maximum rate of 2 microseconds per conversion. This fast settling and digitization by encoding process allows a typical computing throughput rate of 476,190 channels per second, including settling time. The sampling frequency is provided by a General Radio

27

Decade Oscillator, via a locally developed sampling circuit. The stability of the oscillator is 0.001% of indicated value.

3. Texas Instruments Silent Electronic Data Terminal, Model 733

The TI 733 consists of a keyboard used as a printer, a programming input/output control device, and a transmit/ receive device interfaced with a peripheral, dual disk, drive unit. The system provides rapid, highly accurate processing and was primarily used for both time and frequency domain analysis. The frequency domain analysis was effected by standard Fast Fourier Transform techniques.

4. Orbis Model 76 Diskette Drive

The Orbis Model 76 is a compact, portable, dual drive, direct access, 256 thousand byte floppy disc data storage device. The floppy magnetic discs provided the capability of long term storage of vast quantities of data for later analysis.

C. EQUIPMENT LIST

The following is a list of the equipment used during the course of the investigation. Also, the abbreviated name of each piece of equipment is listed as it will be referred to throughout the text.

TABLE I

EQUIPMENT LIST

Description	Abbreviation
Scope	Tecktronic Type 551 Dual-Beam Oscilloscope
Frequency Synthesizer	General Radio 1312 Decade Oscillator
Timing Simulator	Interface Technology Timing Simulator/Word Generator, Model RS-648
Frequency Counter	Hewlett Packard Model 5223L Electronic Counter
Filter HP	Krohn-Hite Frequency Filter, Model 3342
Filter BP	Krohn-Hite Frequency Filter, Model 3322
PAR Amplifier	Princeton Applied Research Amplifier, Model 113
MIC Power Supply	Bruel and Kjaer Microphone Power Supply, Model 2804
ARB	Wavetek Arbitrary Waveform Generator, Model 175
MIC Preamp	Bruel and Kjaer Model 2619
Power Supplies	Hewlett Packard Model 721A
Power Amplifier	Kilowatt Amplifier Model L2 Instruments, Inc.
Oscilloscope	Hewlett Packard Model 140A Oscilloscope
Nicolett	NSC 660B Dual Channel FFT Analyzer

29
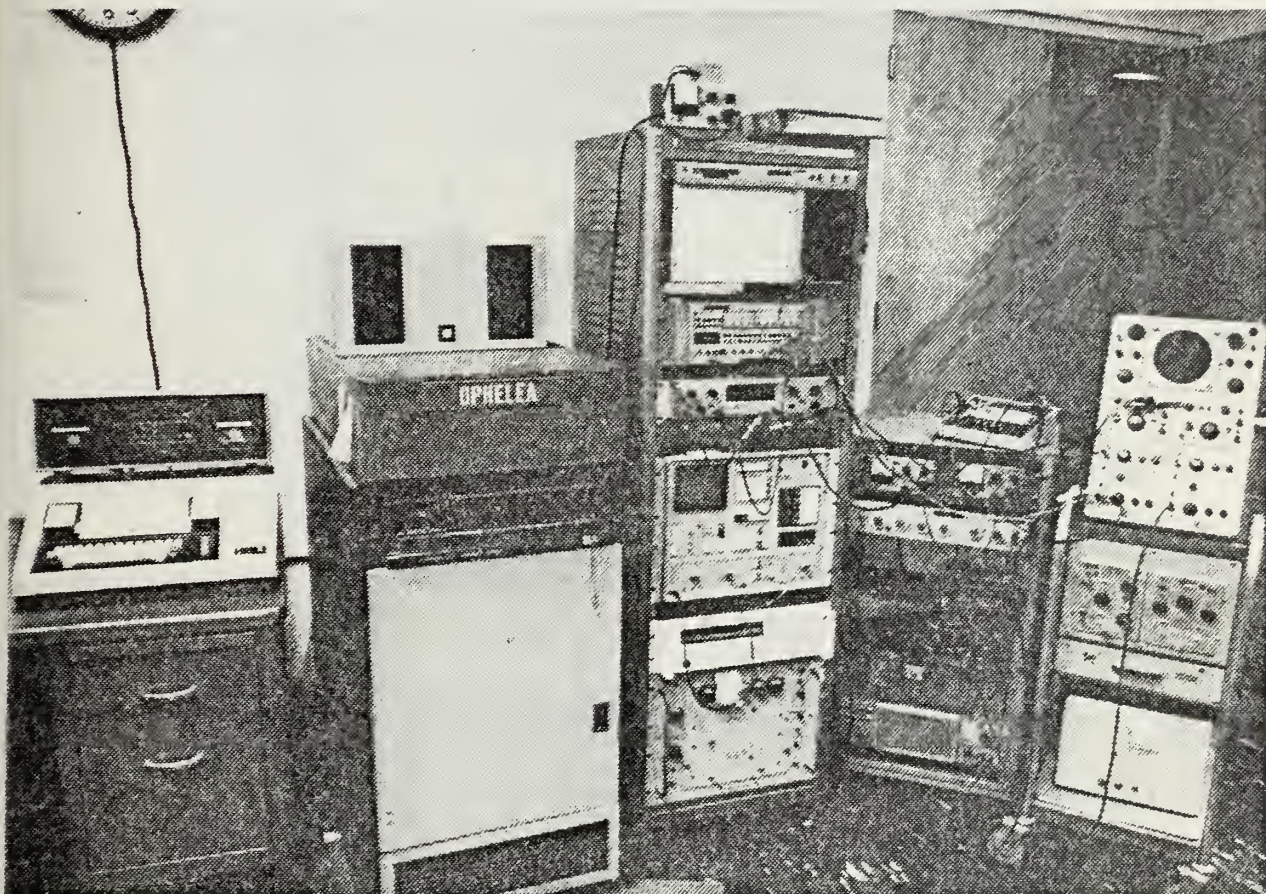
FIGURE 5. Ocean physics laboratory equipment

30
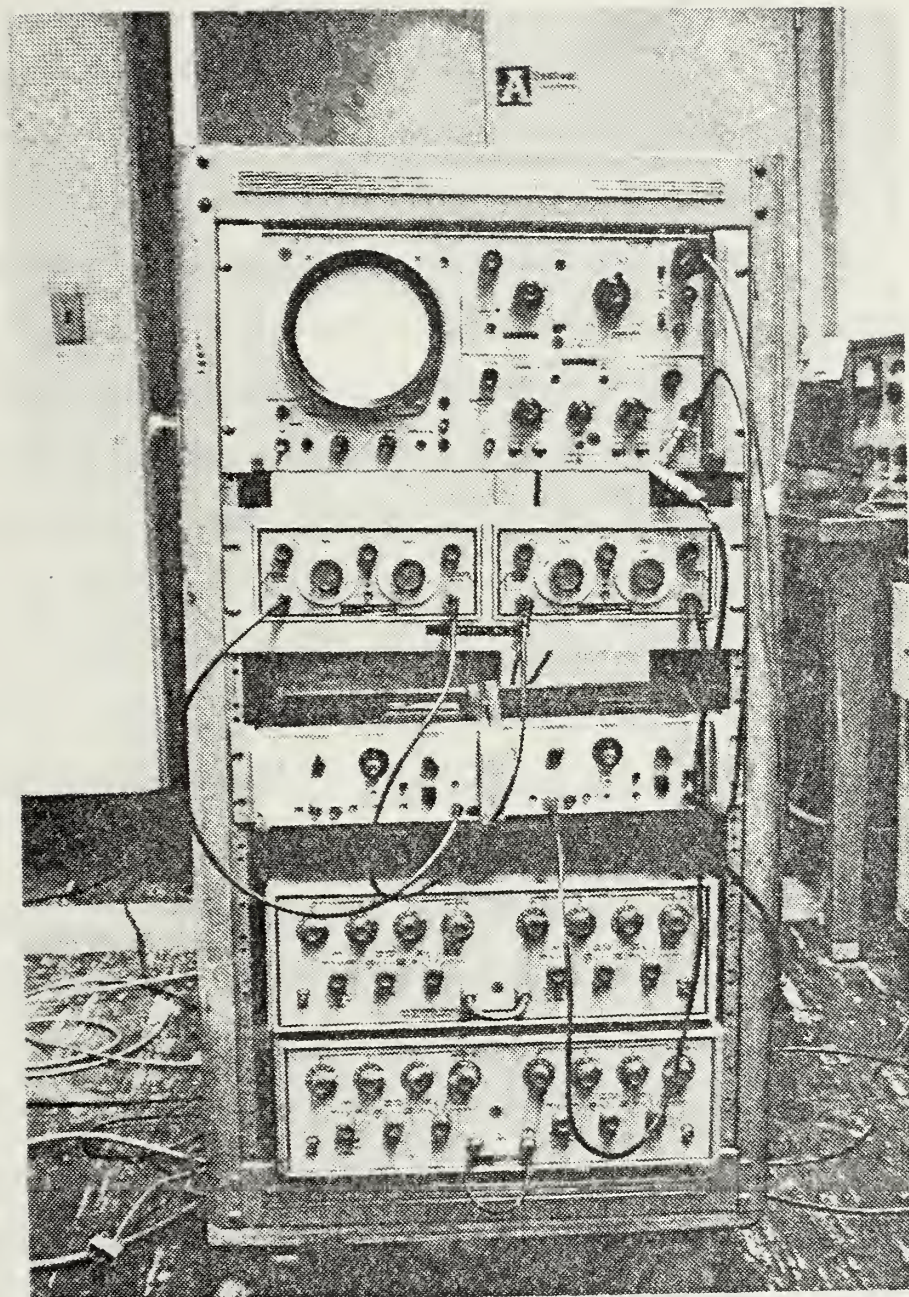
FIGURE 6. Anechoic chamber equipment

31

IV. EXPERIMENTAL APPARATUS AND PROCEDURES

A. SEAMOUNT

The physical models used for this investigation were the same ones Spaulding used in 1979 [Ref. 19]. They were of differing levels of complexity. The simpler of the two, the 2D (PE Contour), was constructed using a technique similar to that used in the fabrication of aircraft wings [Ref. 20]. It conformed to the profile of Dickens Seamount along track 6 of the ocean traversed by Ebbeson [Ref. 21].

This model had the profile of the seamount along track 6 but had none of the variation of the real seamount in a direction perpendicular to track 6. As such, this model represented a physical manifestation of the 2D, parabolic equation computer model used by Jensen [Ref. 22].

The more complex of the two models, the 3 dimensional scale model of Dickens Seamount, was also constructed for Spaulding in 1979 [Ref. 23]. This model was constructed by Modelmakers, Inc., of San Francisco to conform to the bathymetric data supplied by Ebbeson. The seamount model was constructed by laminating 1/8 in layers of particle board cut to represent the shape of the real Dickens Seamount as accurately as possible at the appropriate depth. The result, to this stage in construction, was what would appear to be a contour

32

map of the seamount if it were viewed from overhead. Once
all layers were completed and assembled in the appropriate
sequence, the entire structure was covered by a thin layer
of plaster to smooth the transition from layer to layer and
to add surface density to the model. The final result was
a three dimensional, acoustically rigid, scale model that
accurately reflected the known bathymetry of Dickens Seamount
to a resolution of what would correspond to 25 m at sea. The
scale used was 5 inches to represent 1 km or 1:7874.

B. RANDOMLY ROUGH PLANE SURFACE

Three randomly rough surfaces were constructed of aluminum
plates covered with pea gravel. The plates were 48 inches
by 60.75 inches, 48 inches by 48 inches, and 19.7 inches by
19.7 inches. The 48 inch by 60.75 inch surface was used to
model a randomly rough ocean above the model of Dickens
Seamount. The 48 inch by 48 inch surface was used to extend
the work done by Bailie [Ref. 22] for a surface of hemispheri-
cal bosses to the case of a randomly rough plane surface.
The 19.7 inch by 19.7 inch surface fitted with a height
measuring micrometer and track was used to investigate the
statistics of these surfaces.

The construction procedures were very straightforward.
The surface involved was covered with melted paraffin to a
depth of approximately 0.5 cm. Paraffin was chosen because
of its ease in application and low melting point. As Hollis
pointed out [Ref. 24], the paraffin serves much better than

33

other materials because of the ease with which one can eliminate bubbles in the substance and thus avoid the problem of bubble resonances. After the paraffin had cooled a short time, pea gravel was added until a relatively thick layer that completely covered the paraffin was achieved. Then, using a hand-held hot air blower, the surface was reheated until the paraffin began to melt. As the paraffin melted, the gravel would sink down into it. Thus after the paraffin had cooled a second time, the gravel was securely imbedded in it and therefore attached to the aluminum plate. After the entire plate was cooled a second time, touch up additions were made to any area in the gravel surface where a significant amount of paraffin was visible. When the procedure was complete, there was no area on any of the three plates where the presence of the gravel was not the dominant feature of the surface.

As the purpose of each of the plates was different, so were the details of each plate before the gravel was applied. The plate to be used to model the ocean surface was 48 in by 60.75 in. The gravel surface itself covered an area of 45 in by 55 in on this plate. After the gravel was applied, the model ocean was then bolted to a supporting frame to minimize curvature when suspended and reduce the effort required to move it. Then the plate was suspended at a height appropriate to the scaling of the seamount using a chain fall. A detailed look at the specific appearance of this model ocean

while in place above the seamount is contained in Figures 7 and 8.

The plate to be used for boundary wave investigation was 48 inches by 48 inches. In the center of the plate a hole 1.5 inches in diameter was drilled to admit the source. Then holes 0.32 cm in diameter were drilled at ranges of 10 cm, 20 cm, 30 cm, and 40 cm from the source hole along one radius. This drilling procedure was repeated along radii that were separated by 15 degrees in a complete circle around the source hole. Thus there were a total of 96 holes of 0.32 cm diameter in the plate surrounding the source hole. The holes were plugged from the under side of the plate and gravel applied to the upper side. The details of the appearance of this plate with source and receiver in place are contained in Figures 9 and 10.

The sample plate used for statistical study measured 50 cm by 50 cm. After the gravel was applied to this plate, it was installed in a locally designed apparatus to measure the surface characteristics. This device was constructed to allow the placement of a depth micrometer anywhere in the x-y plane. A 5 cm by 5 cm area was then chosen as representative of the entire plate and the depth measured at intervals of 1 mm. These data were formed into a square matrix containing 2600 elements from which the probability density of the heights and slopes were calculated. As can be seen in Figures 11 and 12, the probability density functions for both the heights and
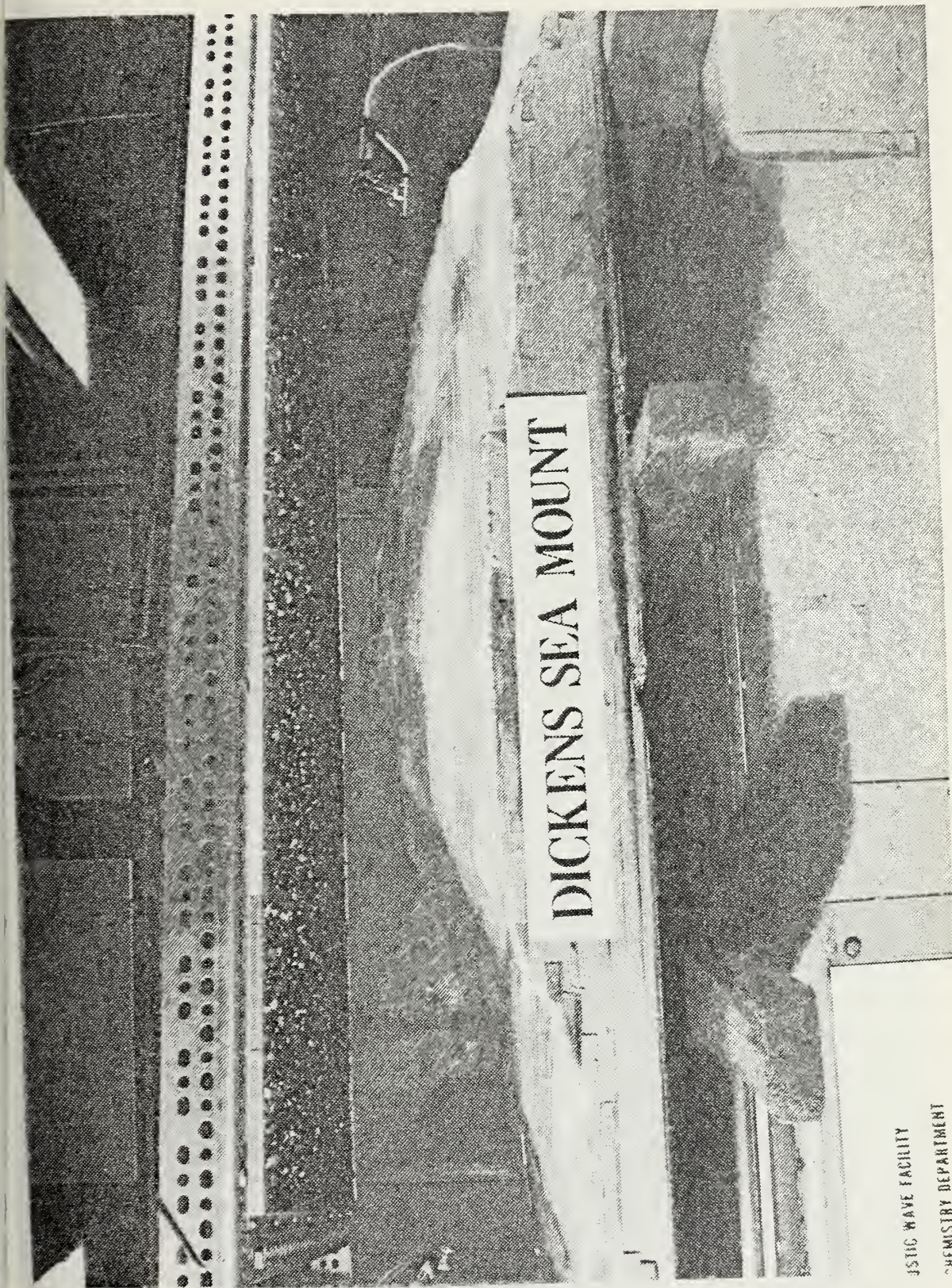
FIGURE 7. Seamount with model ocean in place

36
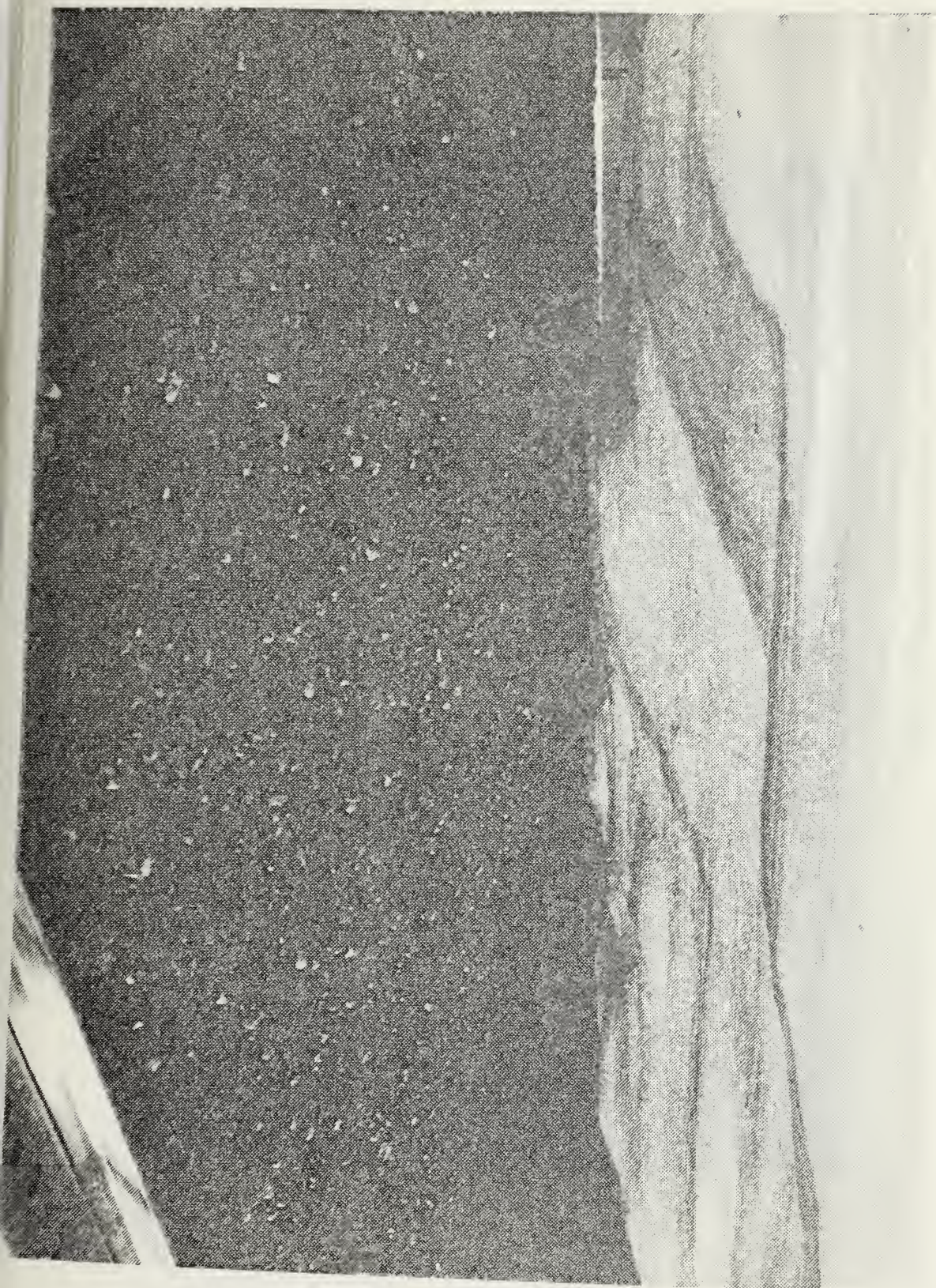
FIGURE 8. Upslope side of seamount model with model ocean in place
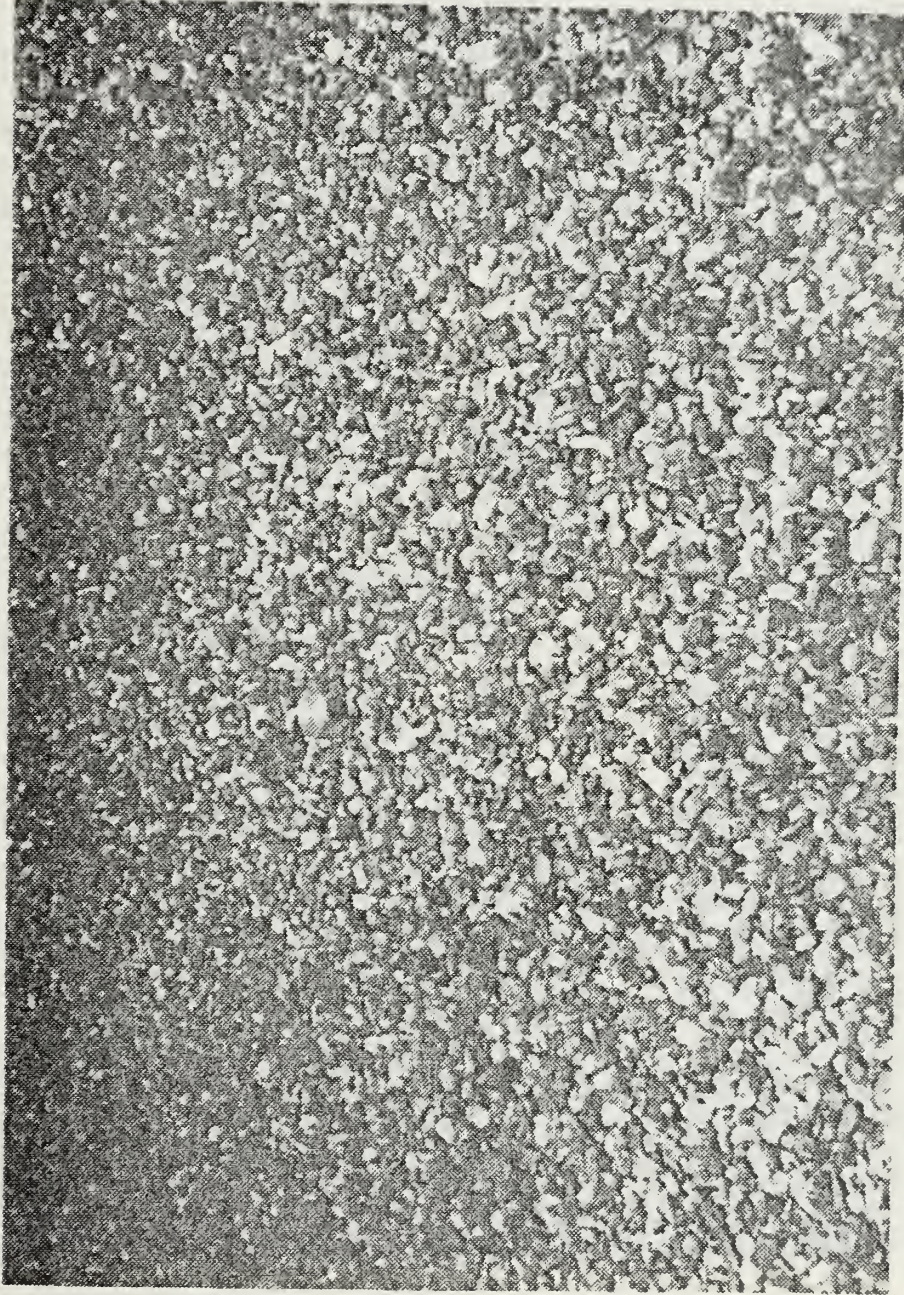
FIGURE 9. Randomly rough plane surface, gravel side
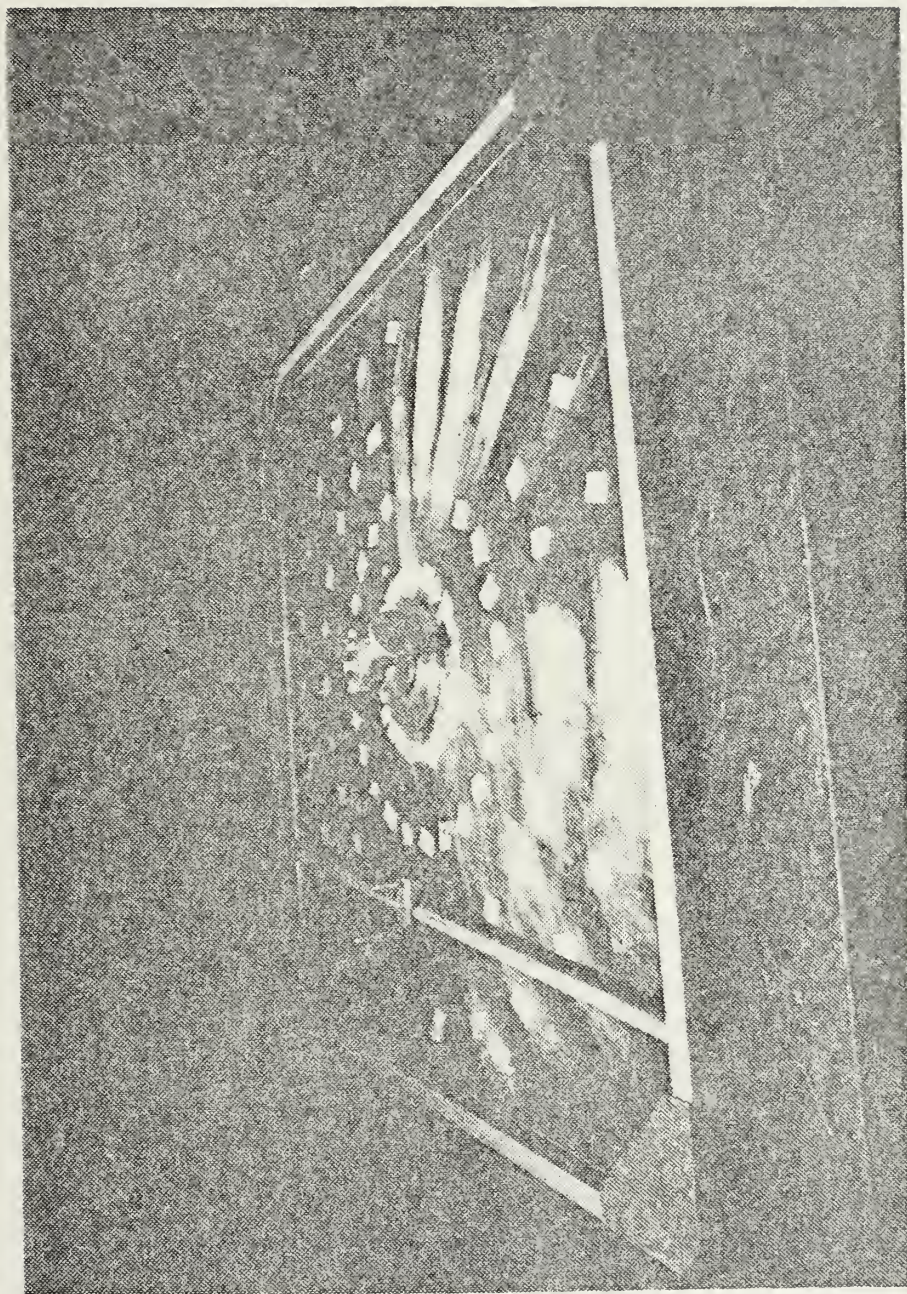
FIGURE 10. Randomly rough plane surface, control side

SURFACE HEIGHT PROBABILITY DENSITY FUNCTION

FIGURE 11

40

SURFACE SLOPE PROBABILITY DENSITY FUNCTION

FIGURE 12

41
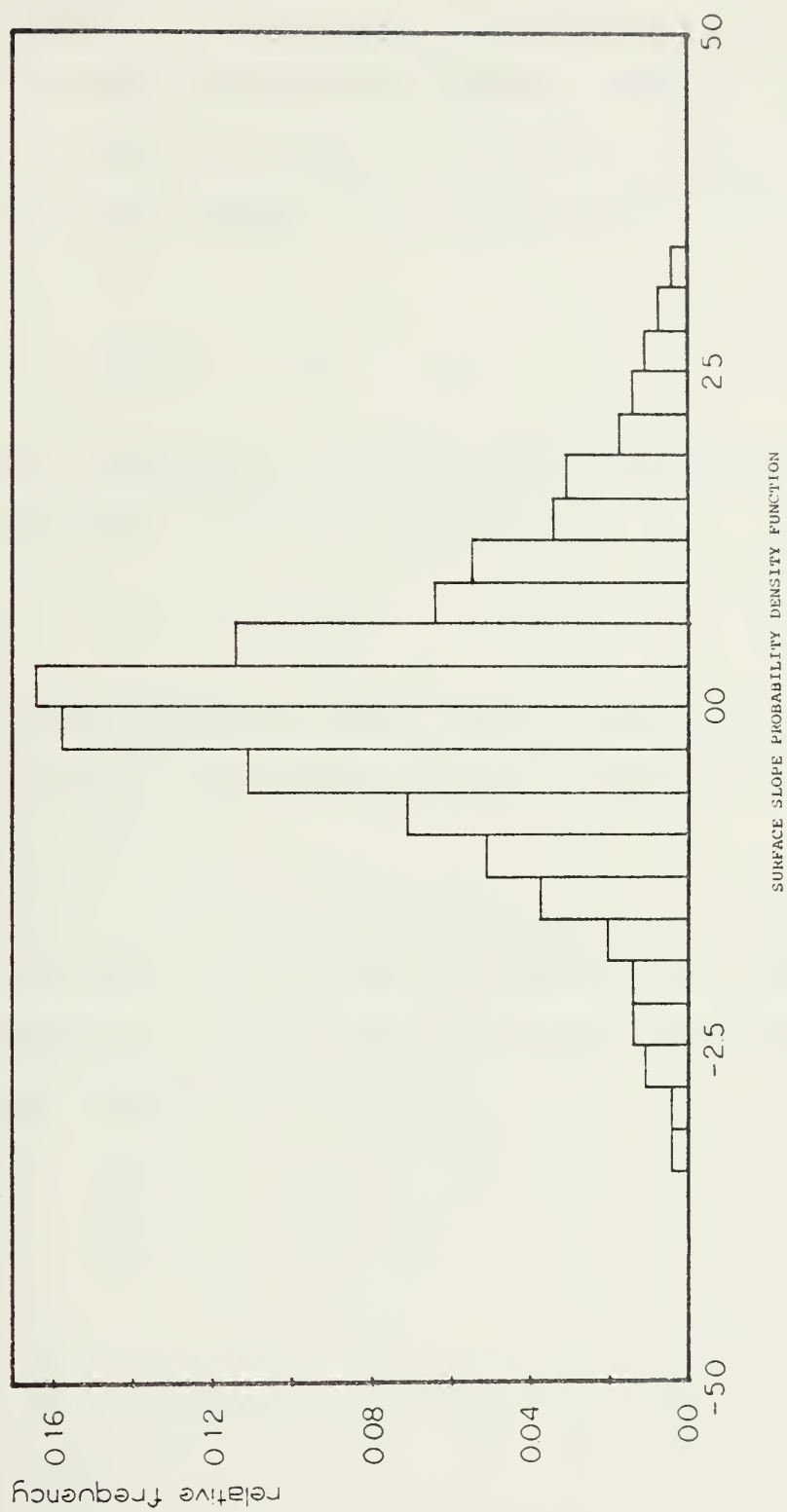
slopes are very nearly Gaussian. The rms height was calcu-
lated to be 2.23 mm and the rms slope was calculated to be
1.15. The correlation function was calculated by row and by
column. This was done for each row/column; then the average
taken. Figure 13 shows the plot of the results of the aver-
age for both rows and columns. If a correlation length is
defined as

$$C(L) = e^{-1} \qquad (25)$$

then the spatial correlation length of this randomly rough
surface, and therefore all three plates, is

$$L = 4.8 \text{ mm} \qquad (26)$$

As can be seen from Figure 13, over this distance there is
virtually no difference between correlation lengths as calcu-
lated by row or by column.

To validate the use of this surface to model the ocean
surface we assume that the 35 knot wind during the ocean
experiment generated a Pierson-Moskovitz wind/wave spectrum
[Ref. 25]. That semi-empirical spectrum is

$$\hat{\phi}(\Omega) = \frac{\alpha g^2}{\Omega^5} \exp[-\beta(\frac{\Omega_0}{\Omega})^4] \qquad (27)$$

where

$$\alpha = 8.1 \times 10^{-3}$$

$$\beta = 0.74$$

.

42

AVERAGE SPATIAL CORRELATION FUNCTION

FIGURE 13

o By Row
□ By Column

centimeters
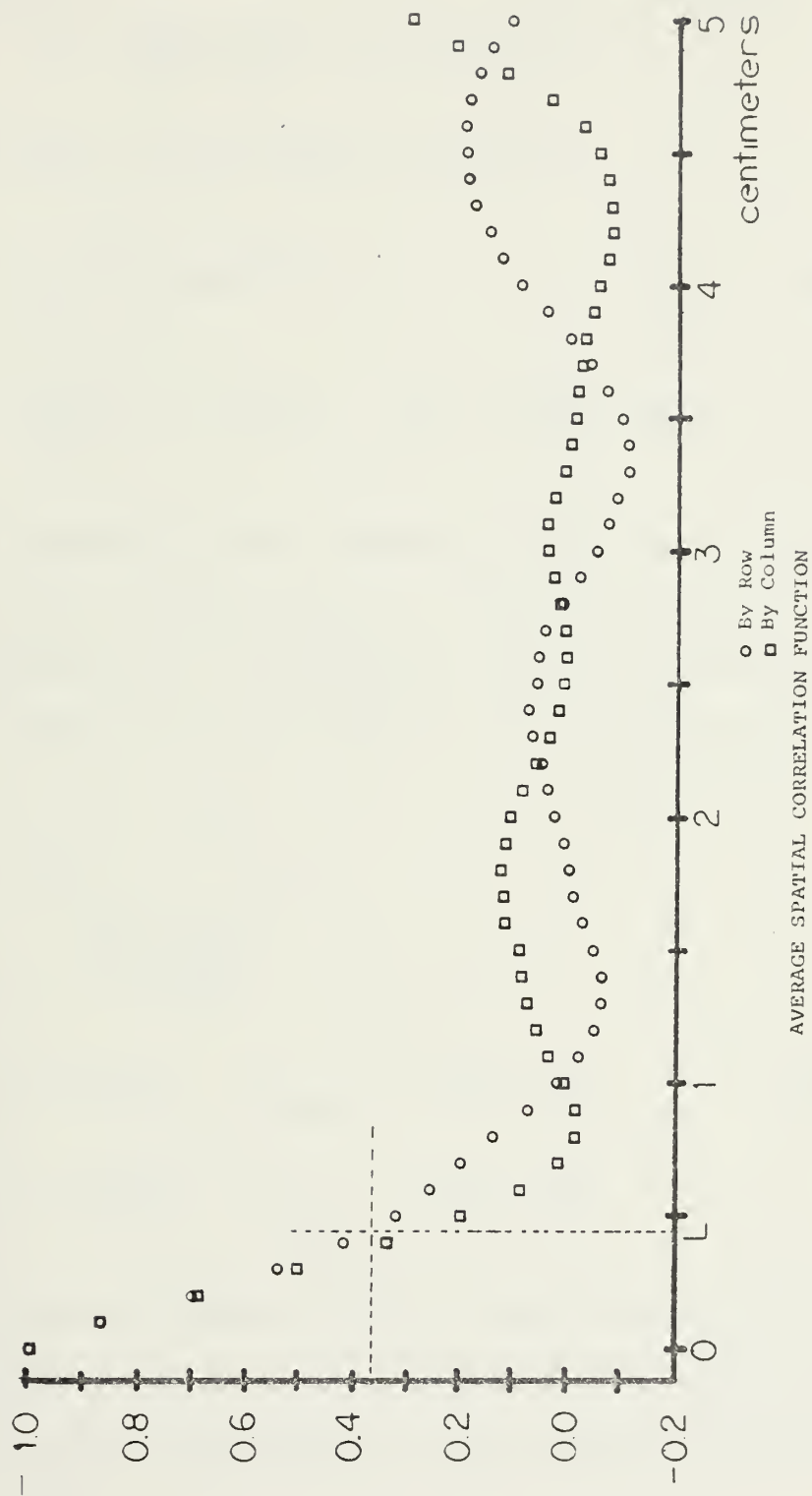
43

$$\Omega_0 \quad = \quad g/W_{19.5}$$

$$W_{19.5} \quad = \quad \text{Wind speed at 19.5 mm above surface}$$

$$g \quad = \quad \text{acceleration due to gravity.}$$

Then the rms height of the waves is given by

$$\sigma \quad = \quad [\int_0^\infty \phi(\Omega) d\Omega]^{1/2} \tag{28}$$

$$= \quad \frac{\alpha \, W^4}{4\beta g^2} \quad = \quad 1.74 \text{ m} \quad \text{for} \quad 35 \text{ knot wind}$$

Since the geometry in the laboratory with the seamount model was the same as the geometry at sea during the CW experiments, modeling of the Rayleigh roughness parameter requires only that $k\sigma$ be the same for the two situations.

$$[k\sigma]_{ocean} \quad = \quad [k\sigma]_{lab}$$

$$f_{lab} \quad = \quad \frac{[f\sigma]_{ocean}}{[\sigma]_{lab}}$$

for $\quad f_{ocean} \quad = \quad 50 \text{ Hz} \quad f_{lab} \quad = \quad 18.1 \text{ kHz} \tag{29}$

for $\quad f_{ocean} \quad = \quad 500 \text{ Hz} \quad f_{lab} \quad = \quad 181.3 \text{ kHz}$

It is assumed that the phase shift at the pressure release ocean surface does not have to be modeled in the laboratory surface because of the randomness of the surface scattered signal.

44

C. SOURCE/RECEIVER SELECTION

1. Seamount

Since the objective of the analysis was to extend the work Spaulding has done [Ref. 26] the choice of source/ receiver was made to correspond to that made by him. This choice was also dictated by the ocean experiment of Ebbeson [Ref. 27]. As shown in Figure 14, the bulk of energy [Ref. 28] intersected the source side of Dickens Seamount about midslope. This energy was contained in two major bundles which apparently divided slightly before intersecting the seamount itself. In an effort to duplicate this effect as closely as possible an extended source was used. That is, a low "Q" 8 cm by 9 cm rectangular solid dielectric transducer was selected as the source and a 1/2 inch B and K microphone as the receiver. These were of the same type used by Spaulding during that portion of his procedure [Ref. 29]. The choice of receiver was driven by the twin requirements for both small size, and thus increased high frequency response, and sufficient sensitivity. The choice made was thus the 1/2 inch B and K microphone, its associated preamplifier and power supply. In some ways, this choice of source was unfortunate, as it was later discovered, since this type of source proved to be unstable both in time and in frequency. The variability shown in Figures 15 through 18 demonstrate the magnitude of the problem. The attempts at finding a solution to this problem will be discussed at length in the section dealing with signal processing.
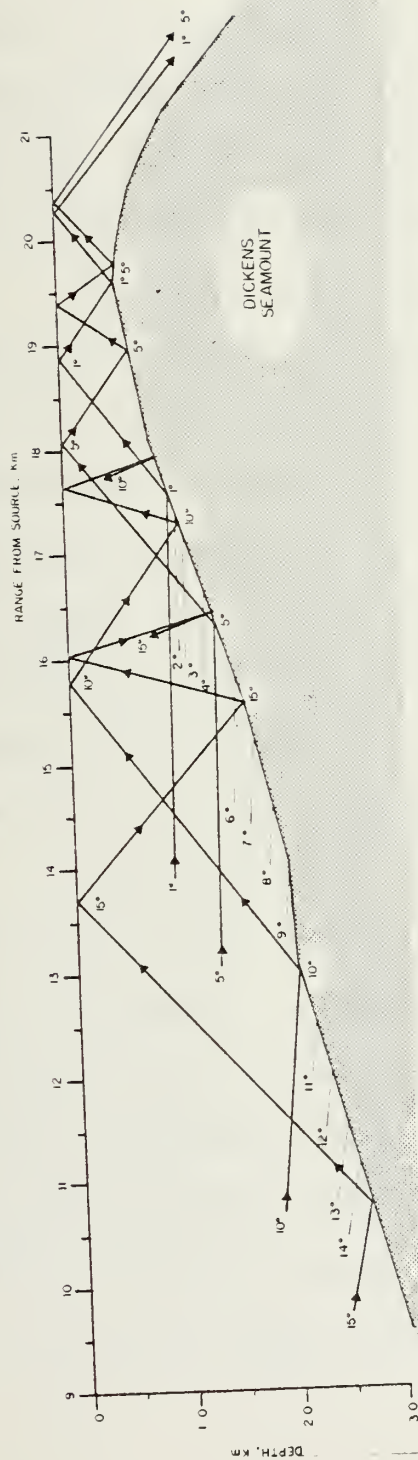
FIGURE 14. Ocean rays that apparently propagate over seamount and source placement to model that propagation

2. Randomly Rough Plane Surface

Equation (24) assumed a point source and point receiver both on the surface. The selection of a source/receiver combination became a tradeoff between size (since $ka << 1$ where a is the radius of the source to approximate a point source) and signal strength. In view of this tradeoff, the B and K Model 4145 one inch diameter microphone was chosen for the source and the 1/2 inch B and K Model 4133 with a 3.2 mm probe tube was chosen for the receiver.

To increase the radiation parallel to the plate the source was mounted in a circular cap 2.5 cm in diameter with a hole 1.3 cm in diameter in the side. The cap was filled with tacky wax to a level and at an angle such that the existence of a standing wave was not possible. The cap itself was part of a larger device that permitted vertical adjustments using a micrometer and rotational adjustments using a compass rose. Figures 9 and 10 show the source, both from the upper and lower sides of the randomly rough plate.

The half inch B and K Model 4133 receiver was attached to a 3.2 mm probe tube that was fitted through a micrometer dial. It also had a nylon spacer between the barrel of the probe tube and the cap that actually fitted to the 1/2 inch B and K microphone itself. This spacer provided electrical isolation between the aluminum plate and the microphone and therefore between the source and receiver. The probe tube was 7.8 cm long from the end of the tube to the nylon spacer.

The small diameter of the probe tube ensured that the receiver was small compared to a half wave length for the highest frequency of interest to avoid pressure averaging over the face of the microphone. This was a potential problem because of the flush mounting of the receiver.

The power supply for the receiver was battery powered. This significantly reduced the electrical noise in the system. Since the heating element was not used, thermal noise was also significantly reduced. Since the height of both source and receiver was set by micrometer, firm control of the relative source/receiver height was obtained. This was important because, as reported by Bailie [Ref. 30] and Hollis [Ref. 31], the boundary wave was sensitive to source height relative to the roughness elements.

D. SIGNAL PROCESSING

   1. Source Signal

      a. Seamount

      Because of the response of the rectangular solid dielectric transducer, a significant amount of experimentation was required to find the most advantageous combination of polarization voltage, driving voltage, and wave form. Fortunately, the Wavetek 175 Arbitrary Waveform Generator (ARB) was designed to provide the flexibility necessary to adequately address these complex problems.

      First it was noticed the wave form produced by the source was fairly sensitive to the polarization voltage

48

applied. This was especially true of the time necessary to insure that the ringing had decayed to a level that could be considered negligible. After several different voltages were examined, the obvious best choice was +150VDC. This produced a signal that was surprisingly free from ringing when considered in the context of the low "Q" of the transducer. The signal, as viewed without obstruction of the seamount is contained in the top graph of Figure 19.

Second, the amplitude of the driving signal was addressed. The problem was considered in the context of getting maximum output from the transducer without overdriving it. Again, after a significant amount of experimentation, a driving voltage of 110 V AC proved to be of shortest duration for the polarization voltage applied.

The third, and probably most difficult, consideration was the actual wave form to be applied to the transducer. At this point in the effort, the tremendous advantages the ARB afforded came to the fore. In addition to several pre-programmed wave forms stored in Read Only Memory (ROM), the ARB also provides several Random Access Memory (RAM) devices. Since the resultant transducer response to the preprogrammed waveforms proved unsatisfactory, several waveforms were programmed in the RAM. Each RAM consists of 256 discrete blocks of memory. The voltage to be applied via the ARB is then programmed by the user in each of these 256 blocks. The voltage is then entered as a quantized level from 0 to ±127.

The actual voltage that is assigned to each quantum level is controlled by the user via the amplitude setting provided. Thus for an amplitude setting of 1 volt, +127 would correspond to +1 volt and -127 would correspond to -1 volt. Using this approach it was observed that the best output from the dielectric transducer was obtained by programming a RAM to apply +127 from the first block, -127 from the second block, 0 from the remaining 254 blocks, setting the amplitude to 0.5 volts, applying a frequency of 1000 Hz to the process; and, finally, amplifying the results to a value of 110 VAC. Therefore the voltage applied to the source was a positive impulse of 110 VAC followed by a negative impulse of -110 VAC. The voltage was actually applied to the source for 7.8 microseconds. This process was repeated every 25 milliseconds. A detailed list of equipment settings is contained in Table II, Appendix A.

  b. Randomly Rough Plane Surface

    In order to be used as an acoustic source, the one inch B and K microphone must first be biased with a DC voltage. Once this has been accomplished, the AC signal is imposed on top of the bias voltage. The B and K Model 4145 one inch microphone is rated by the manufacturer at a voltage of 250 V (peak plus bias) [Ref. 32]. Thus with a bias voltage of +150 VDC an applied AC signal of 100 VAC represents a driving voltage that is as large as possible yet still within the manufacturer's specifications. Therefore, this combination of DC and AC voltages was used.

In an effort to get as much energy in the harmonics of the driving frequency as possible, a half triangular pulse was selected from those preprogrammed in the Wavetek Arbitrary Waveform Generator (ARB). This pulse was driven at a fundamental frequency of 2.5 kHz. This gave a frequency spectrum with relatively significant amounts of energy at frequencies that greatly exceeded $kL \leq 1$, where L is the spatial correlation length of the gravel surface.

2. Received Signal Processing

a. Seamount

With the two models of Dickens Seamount in the Ocean Physics Laboratory, an increase in the signal to noise ratio was achieved by taking 1500 samples of each signal being considered. Since, for N samples of a signal in the presence of noise

$$\Delta\left(\frac{S}{n}\right) = 10 \log \sqrt{N} \qquad (30)$$

Thus, for 1500 averages a gain of 16 dB was achieved in the signal to noise ratio.

A second consideration that needed to be resolved before actual data taking began was that of the sampling frequency. As stated by the uniform sampling theorem, if any signal which is band limited is sampled in time, with a uniform intersample period T_s such that

$$T_s \leq \frac{1}{2W} \qquad (31)$$

51

where

$$W \quad = \quad \text{Bandwidth}$$

the signal is completely specified [Ref. 33]. This leads to
the result

$$f_s \quad \geq \quad \frac{1}{T_s} \quad \geq \quad 2W \qquad\qquad (32)$$

But, given reality, if a figure of 3W is used rather than 2W,
the data collected is much more reliable. Since the highest
sampling frequency with which the A/D equipment could deal was
320 kHz, this would allow reliable frequency data up to
approximately 100 kHz.

Therefore, using a sampling frequency of 320 kHz,
1500 averages, and a pulse repetition rate of 25 milliseconds,
the data from the 2D (PE Contour) and the scale model Seamounts
were collected and stored on magnetic disk for later processing.
These recorded signals were of both seamount models without
ocean, both seamount models with mirror ocean, and 21 runs
for both models with rough ocean. Since the spacial correla-
tion length had been established, L = 0.48 cm, by shifting
the position of the ocean above the seamount model a statis-
tically "new" ocean had, in effect, been placed over the model.
By shifting the ocean that had originally been centered over
track 6 ± 10 cm in 1 cm increments, 21 statistically indepen-
dent manifestations of the randomly rough ocean had been
placed over the model. This allowed statistical methods to

52

be used to arrive at an average pressure as a function of both time and frequency.

It was during the taking of the data with the rough ocean in place above the scale model seamount that possible problems with the source became apparent. While observing the plot of pressure versus time a change in level as a function of run number was noticed. Since the first peak in amplitude of the received signal was entirely due to diffraction, the presence of the ocean should have made no difference in the amplitude of this first peak. The amplitude of the first peak as a function of run number is shown in Figure 15. The entire procedure for all 21 runs took place over a period of approximately four hours. As this figure demonstrates, apparently there was a very low frequency oscillation in the source strength presumably due to instabilities in the source itself. This immediately raised the question of the frequency stability of the source.

With the rough ocean in place above the seamount, the duration of the first peak is represented by somewhat more than 16 data points. Since the algorithm used in the Fast Fourier Transform requires the use of the number of data points such that the number is an exact multiple of 2, the first 16 points of the pressure versus time signal that was above background noise was transformed into the frequency domain. This led to a frequency resolution of 20 kHz. After choosing the case of the 2D (PE Contour) model with the
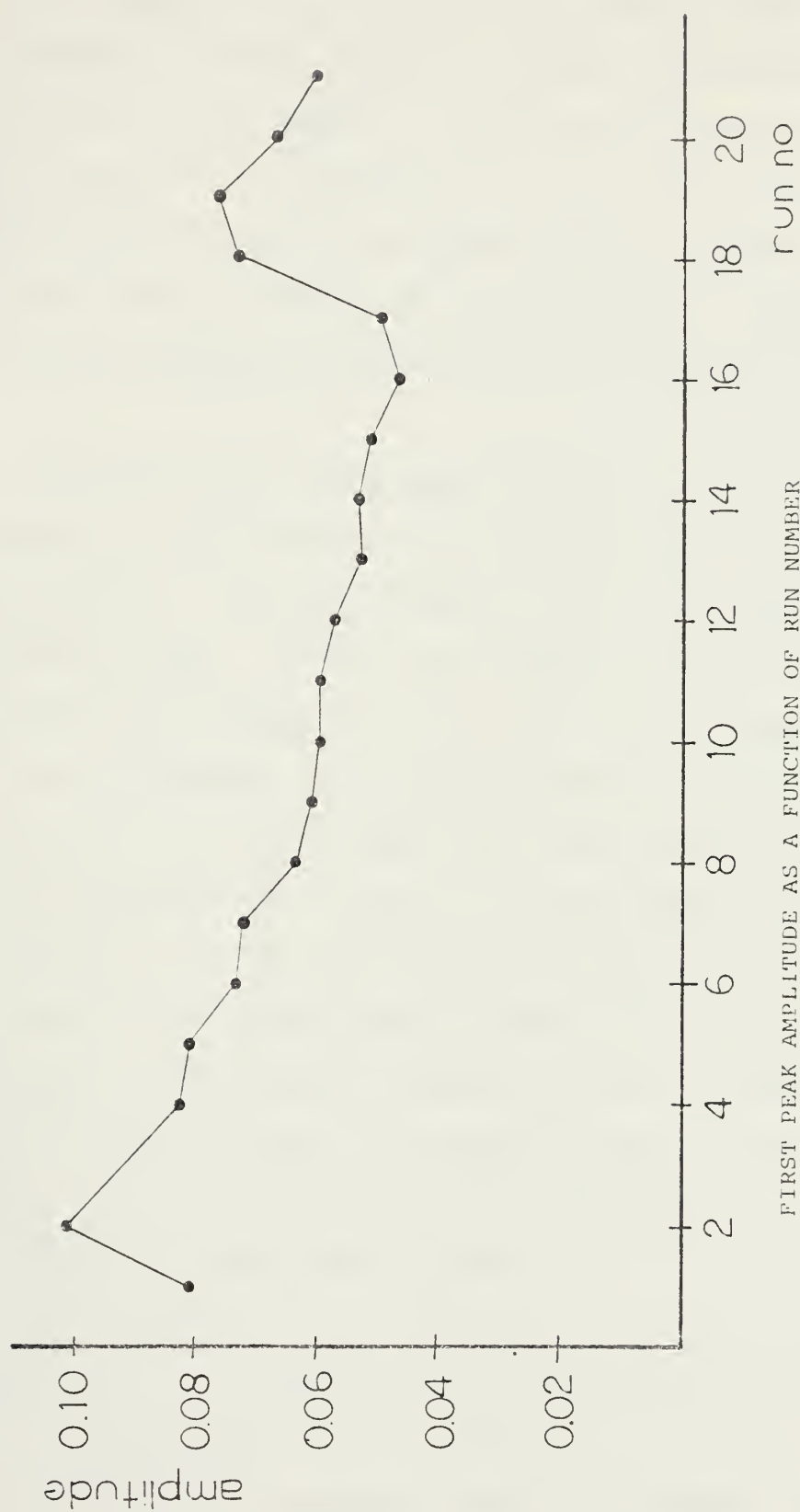
FIRST PEAK AMPLITUDE AS A FUNCTION OF RUN NUMBER

Seamount with rough ocean, horizontal displacement constant

FIGURE 15

smooth ocean an arbitrary reference to which to normalize the frequency data representing the first 16 points of each signal that involved an ocean (rough or smooth) was plotted on the same graph as the reference. The objective was to identify a correction factor to be applied to a particular run based on the frequency behavior of the first amount of energy of that which was known to involve diffraction only. Three examples of this procedure are contained in Figures 16, 17, and 18.

As can be seen from these three figures, the frequency response of the source in the neighborhood of 30 kHz is relatively stable. However, above 40 kHz the variance from run to run was extreme. It was also apparent from the behavior of Spaulding's frequency plots that the far-field of the system was not reached until approximately 50 kHz. Based on the foregoing, it was concluded that the time data was reliable for approximately 30 kHz but not necessarily for the higher frequencies. It was concluded that any information about the effect of an ocean above a model of the seamount and its effects on the acoustic shadowing by that seamount would have to be derived from the pressure versus time data. Thus attempts at frequency analysis were abandoned.

b. Randomly Rough Plane Surface

As reported by Bailie [Ref. 34] and Hollis [Ref. 35], the generation of a boundary wave as predicted by Equation (24) is very sensitive to the height of the source relative to the plane of the roughness elements; although less

55

FIGURE 16

FIGURE 17

□ 2D (PE Contour) Rough Ocean
Horizontal Displacement = 0 cm

○ 2D (PE Contour) Smooth Ocean, Reference

FREQUENCY SPECTRUM OF FIRST 50 MICROSECONDS

57

FIGURE 18

□ 3D (Scale Model) Rough Ocean
Horizontal Displacement = -5 cm

○ 2D (PE Contour) Smooth Ocean, Reference

FREQUENCY SPECTRUM OF FIRST 50 MICROSECONDS

FREQUENCY, kHz

dB (arbitrary)
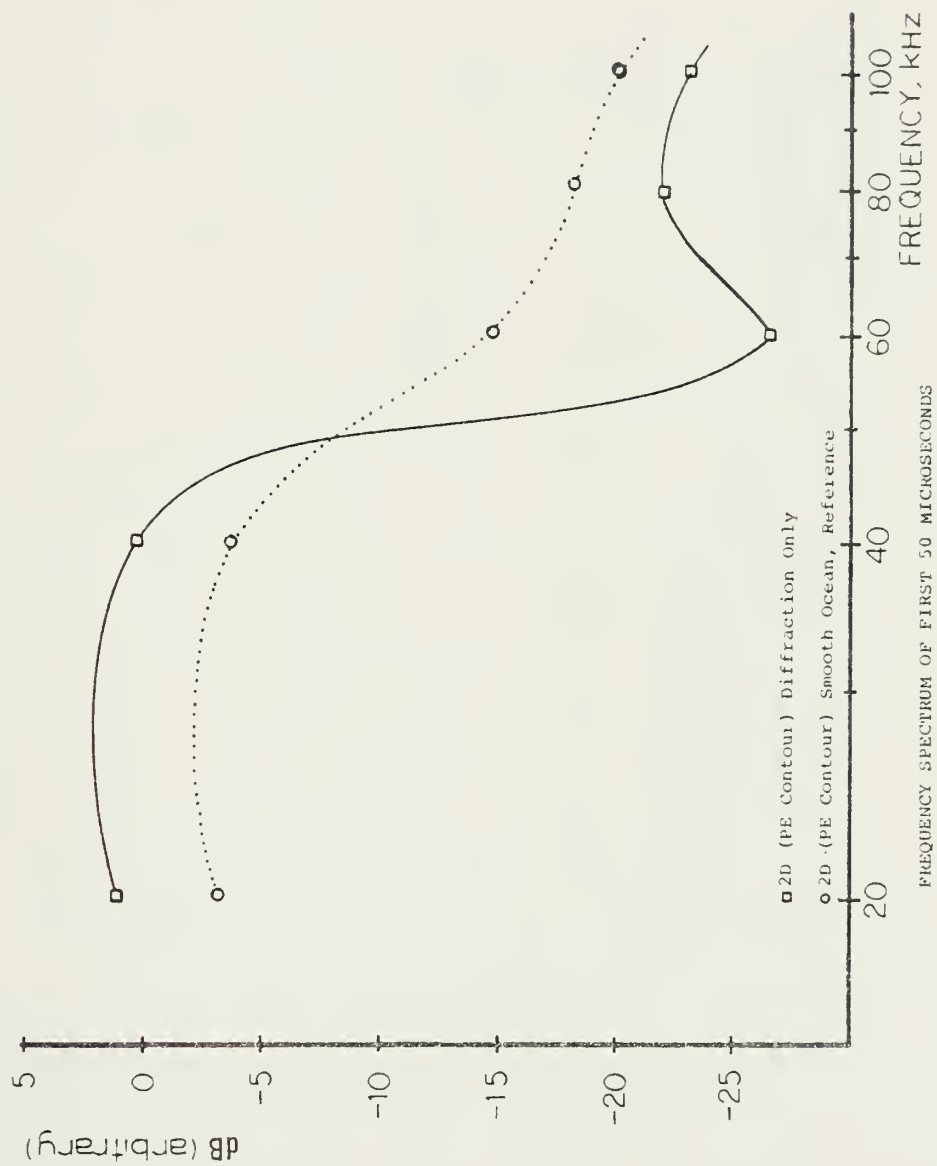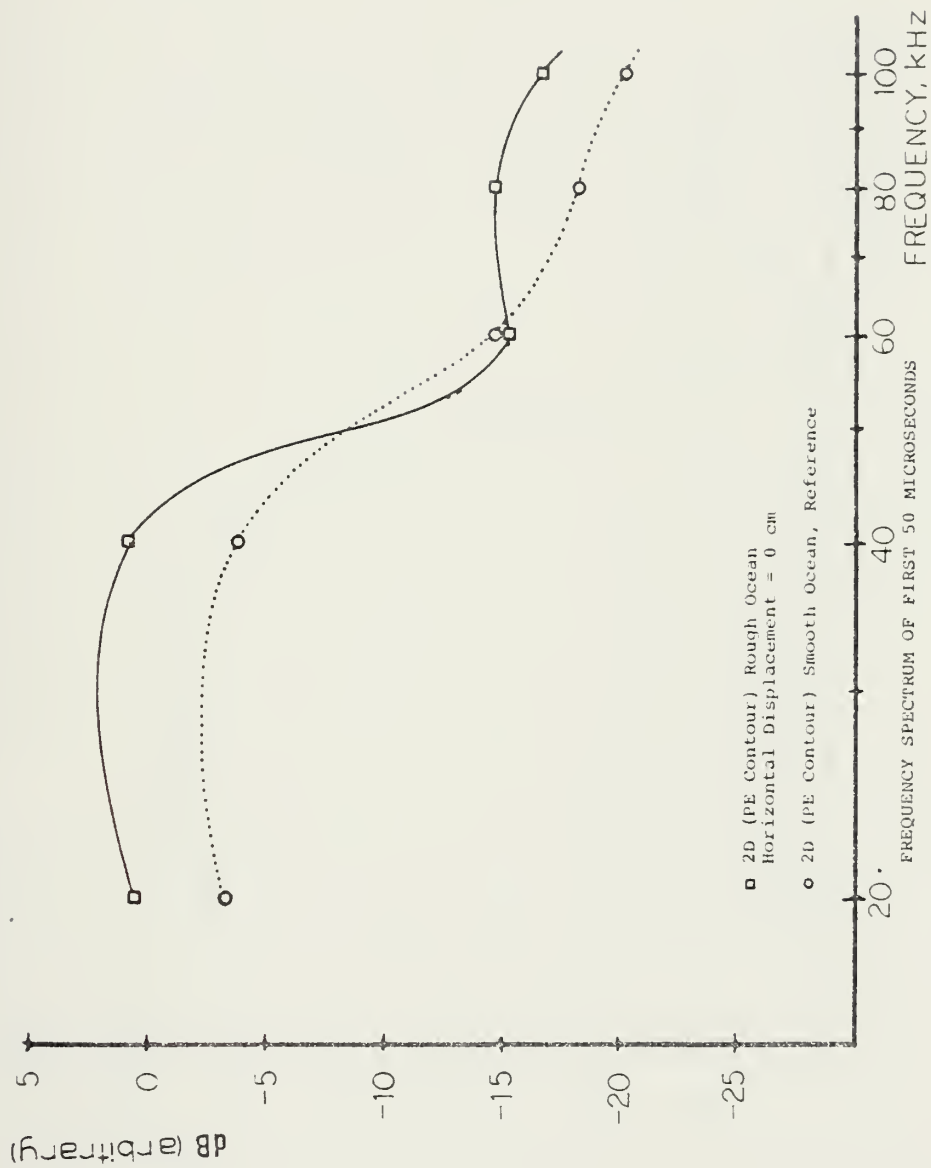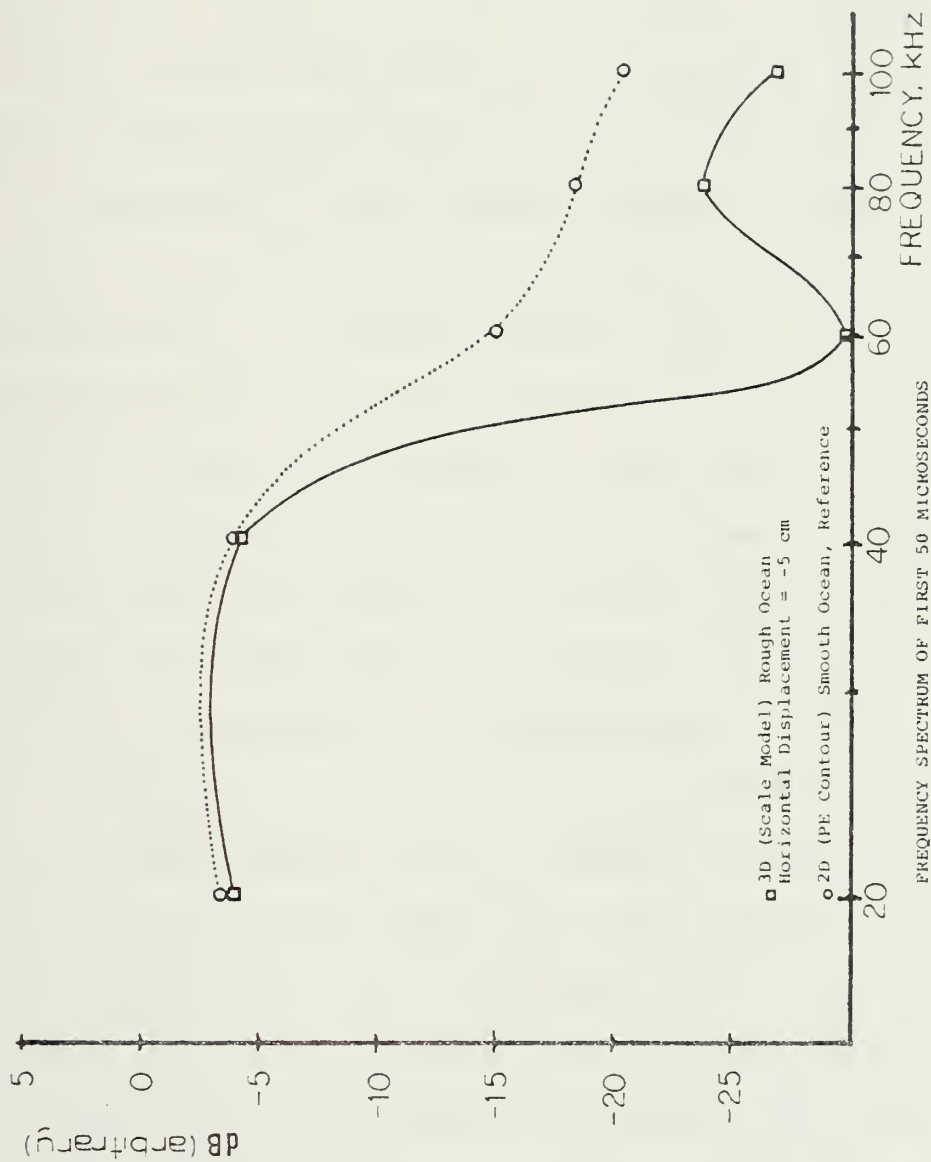
58

so for the relative height of the receiver. A series of
acoustic measurements were made starting with the source
housing height at the upper limit of the mechanism. This
corresponded to a reading on the micrometer dial of 16.84
relative cm. The height of the housing was then decreased
in incremental steps of 1 mm until the top of the hole in the
source cap was completely below the gravel. The maximum
amplitude at each height position is compared to find the
height at which the boundary wave was apparently strongest.
This corresponded to a micrometer reading of 15.84 cm. With
the source set at this height, the receiver was adjusted in
the same manner. It seemed, however, that as long as the
receiver was below the tops of the gravel in the immediate
vicinity but above the midpoint of the gravel; the received
signal was insensitive to receiver adjustment. Therefore,
with the source and receiver set as specified, data collection
began and the heights were not changed regardless of the
variation of the gravel at any particular location.

Each run consisted of the average of 2000 pings
at a particular position on the randomly rough plane surface.
The received signal was amplified, then filtered by 2 cascaded
bandpass filters set with a passband of from 500 Hz to 110 kHz.
The upper limit of this passband was established at this value
as a consequence of the sampling frequency being set at 320
kHz. Thus, because of the Nyquist criterion it was felt that
reliable data up to at least 100 kHz could be obtained without

aliasing. The filtered signal was then amplified again to
boost the signal up to a level that was well within the opera-
ting range of the A/D converter. A complete table of equip-
ment settings is contained in Table III, Appendix A. Each
run was transformed to the frequency domain using Fast Fourier
Transform (FFT) techniques and stored on magnetic disk for
later use.

The use of the probe tube limited the amount of
useful data contained in each signal. Since the probe tube
was 7.8 cm in length, the first evidence of the standing wave
that was generated within the tube occurred at approximately
450 microseconds after the beginning of the receiver's response
to the acoustic signal. This left only 145 usable samples at
a sampling frequency of 320 kHz. Since the algorithm for the
FFT used for processing required the use of the number of
data points which identically equal to a power of 2, the number
of data points used for the FFT was 128. This established the
frequency resolution, Δf, as

$$\Delta f = \frac{sampling\ frequency}{number\ of\ samples} = \frac{320,000}{128} = 2.5\ kHz \qquad (32)$$

Once an arbitrary radial line was designated as
the zero angle, data were taken at the 40 cm and 20 cm range
positions for angles

$$\theta = \theta° + n\ 30° \qquad n = 0,1,2,\ldots,11 \qquad (33)$$

At the 30 cm and 10 cm range positions, data were taken for angles

$$\theta = 15° + n \, 30° \qquad n = 0,1,2,\ldots,11 \qquad (34)$$

Once these rough plate data were obtained, reference data were collected using a smooth aluminum plate with the receiver and the bottom of the hole in the source cap flush with the surface of the plate. Reference data were taken at 10 cm, 20 cm, 30 cm, and 40 cm. These reference data constituted the spherically spreading volume wave needed to calculate the boundary wave ratio as expressed in Equation (24).

To calculate the boundary wave amplitude, both rough plate and smooth plate data were converted into rectangular components for each frequency (magnitude and phase) at each range. Thus, for a particular range and frequency on the rough plate

$$f_R = A_R e^{i\phi_R} \qquad f_R = \alpha_R + i\beta_R \qquad (35)$$

And for the same range and frequency on the smooth plate

$$f_S = A_S e^{i\phi_S} \qquad f_S = \alpha_S + i\beta_S \qquad (36)$$

The boundary wave is computed at that frequency and range

$$f_B = (\alpha_R - \alpha_S) + i(\beta_R - \beta_S) \qquad f_B = A_B e^{i\phi_B}$$

where

$$A_B = [(\alpha_R - \alpha_S) + (\beta_R - \beta_S)]^{1/2} \qquad (37)$$

and

$$\phi_B = \tan^{-1} \left[\frac{(\beta_R - \beta_S)}{(\alpha_R - \alpha_S)} \right]^{1/2}$$

Therefore, the ratio of the rough plate frequency amplitude to the smooth plate frequency amplitude at a particular range is

$$\frac{P_{BWA}}{P_{VWA}} = \frac{A_B e^{i\phi_B}}{A_S e^{i\phi_S}} = \frac{A_B}{A_S} e^{i(\phi_B - \phi_S)} \qquad (38)$$

This is the value to be compared with the predictions as outlined in Equation (24). This ratio was calculated for each range, angle, and frequency and stored on magnetic disk for comparison with theory.

V. EXPERIMENTAL RESULTS AND ANALYSIS

A. SEAMOUNT

Figures 19 through 21 are plots of pressure versus time for various configurations of seamount/ocean modeling. The top graph of Figure 19 is the free field pressure issued by the source, with a duration of approximately 0.15 milliseconds.

The field diffracted over the 2D (PE Contour) model is shown in the middle and is weaker than the free field pressure has about the same duration. The pressure diffracted by the 3D seamount model is somewhat greater than for the contour wedge and its shorter duration may be due to destructive interference for the longer paths around the seamount.

The 2D contour model is of interest because it is the physical representation of what the two dimensional parabolic equation assumes in its solution of the problem. Figure 23 shows this approximation to the real world without ocean surface (top), with smooth ocean surface (middle), and with rough ocean surface (bottom). At very short times, up to 50 microseconds, the field is pure diffraction travelling by the shortest path; from 50 microseconds to approximately 200 microseconds analysis reveals that the scatter is by a single reflection from the ocean surface, a situation that does not exist in the real ocean experiment and which is therefore not studied. The analysis of the forward propagated field starts at 203 microseconds and goes on for 400 microseconds.

FREE FIELD PRESSURE

PRESSURE DIFFRACTED OVER 2D (P.E. CONTOUR) MODEL

PRESSURE DIFFRACTED OVER SEAMOUNT MODEL

FIGURE 19. Pressure versus time for free field, 2D (PE contour), and seamount with no ocean

PRESSURE DIFFRACTED OVER 2D (P.E. CONTOUR) MODEL
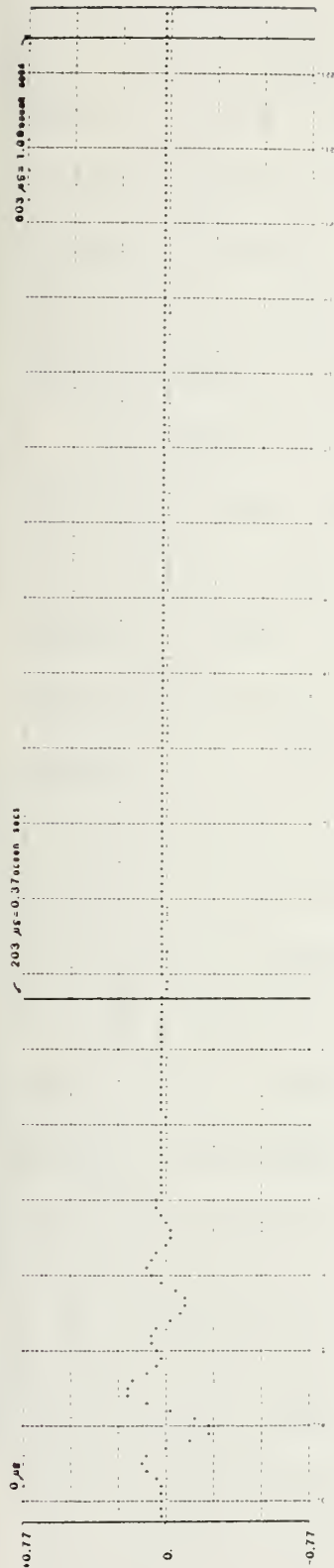
MIRROR OCEAN OVER 2D (P.E. CONTOUR) MODEL

PRESSURE DIFFRACTED AND MULTIPLY REFLECTED

TYPICAL ROUGH OCEAN OVER 2D (P.E. CONTOUR) MODEL
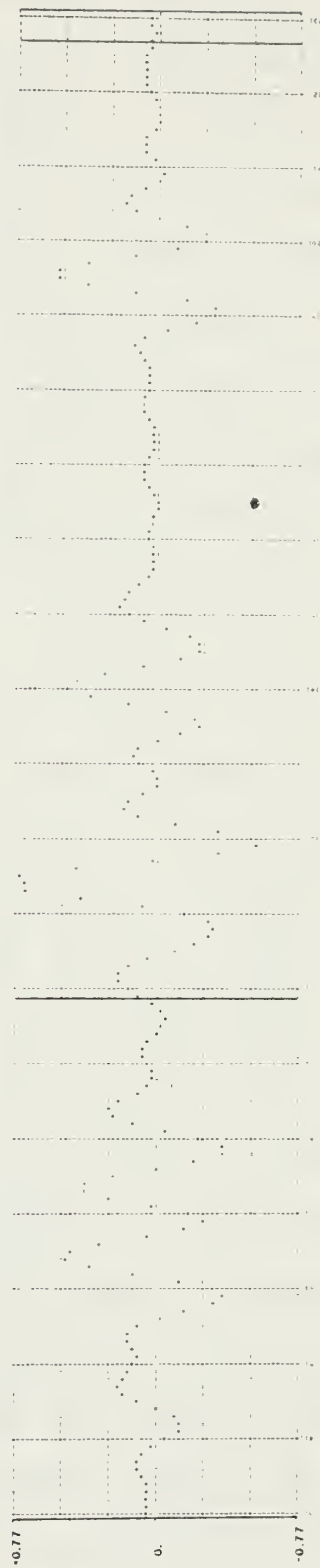
PRESSURE DIFFRACTED AND MULTIPLY SCATTERED
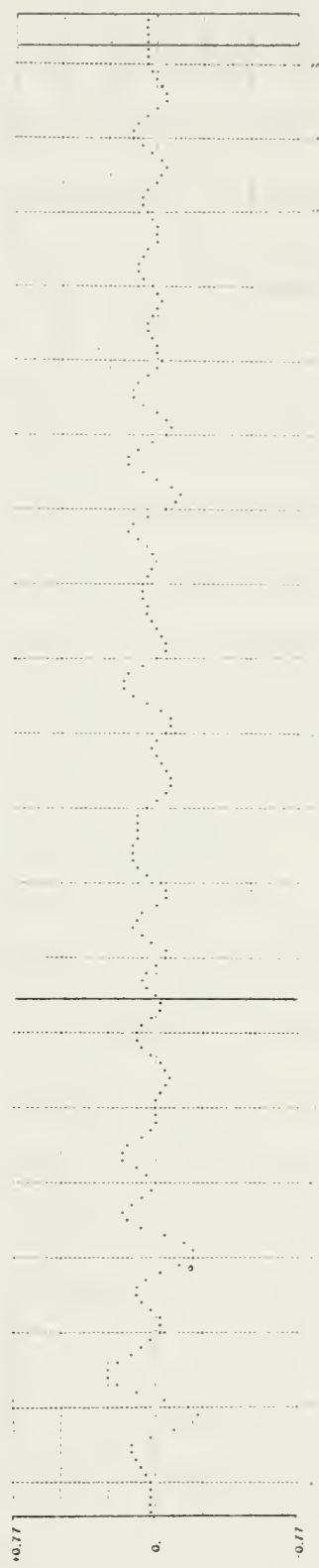
FIGURE 20. Pressure versus time for 2D (PE contour) model, diffracted

65

The ocean equivalent time range is from 0.37 sec to 1.09 sec. Chapman and Ebbeson [Ref. 40] have stated that this is the time between the first and second pulse observed at sea. What is clear from Figure 20 is that a rough ocean causes a significant reduction in this pulse, compared to the smooth ocean situation. This proves; if the ocean surface plays a part in the shadowing by a seamount, that it must be an appropriately rough surface that is assumed in the model.

In Figure 21 the three dimensional model of the seamount is considered. Again, it is the period of this signal from 203 microseconds to 603 microseconds with the purely diffracted signal seen in the top graph, that is of interest. The smooth ocean again causes a very large reverberant signal, compared to the diffracted signal. But this is unrealistic, as the bottom graph shows for the rough ocean surface. The signal for the rough ocean is significantly lower than for the purely diffracted signal. Since the sum of the squares of the pressure amplitudes for each time increment for which the signal is above background noise is proportional to the energy contained in the signal for that time, a comparison of these sums of squares for the purely diffracted signal in the top graph with the signal contained between 203 micro-seconds and 603 microseconds in the bottom graph gives a quantitative feel for the relative amounts of energy involved. For the purely diffracted signal the sum of the squares of the pressure amplitudes was 0.58; whereas, the sum of the

PRESSURE DIFFRACTED OVER SEAMOUNT MODEL

PRESSURE DIFFRACTED AND MULTIPLY REFLECTED
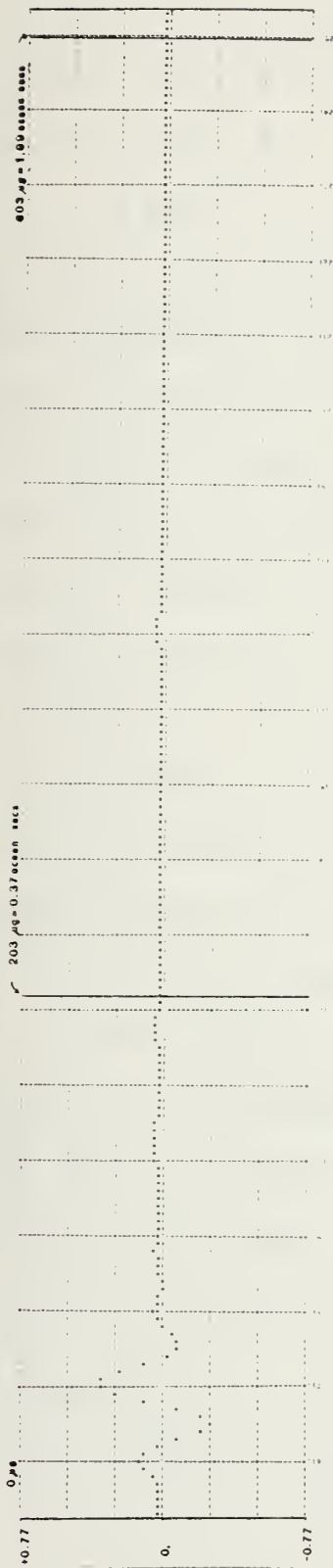
PRESSURE DIFFRACTED AND MULTIPLY SCATTERED
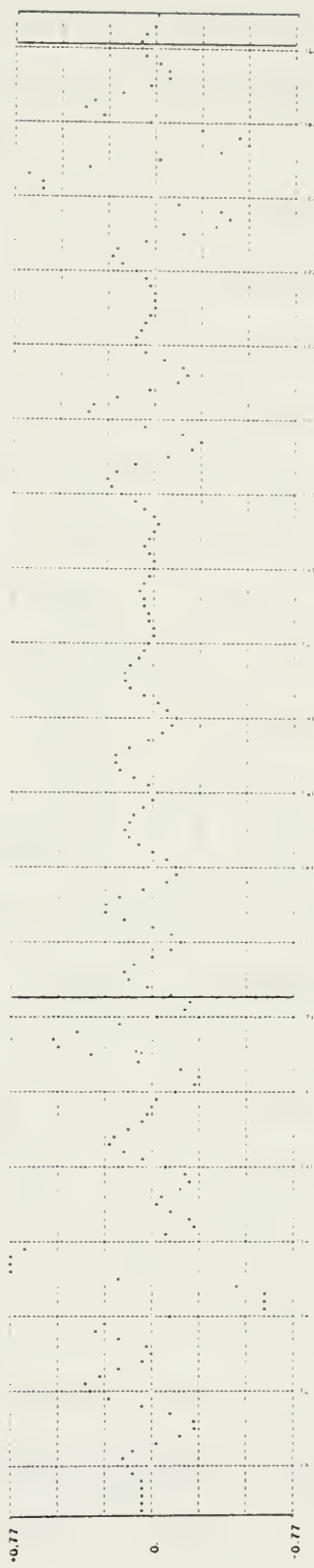
MIRROR OCEAN OVER SEAMOUNT MODEL
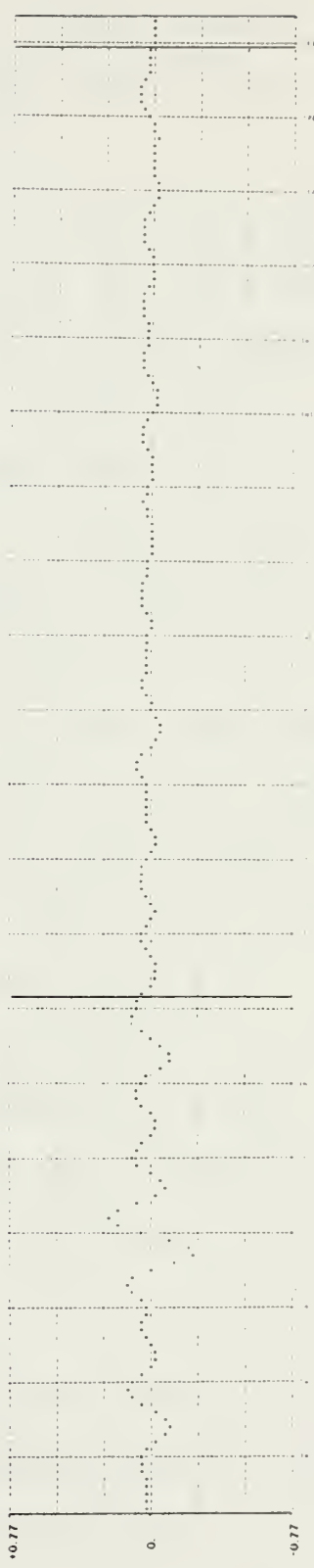
TYPICAL ROUGH OCEAN OVER SEAMOUNT MODEL

FIGURE 21. Pressure versus time for scale model seamount, diffracted, smooth ocean, typical rough ocean

67

squares for the rough ocean pressure amplitudes was 0.34.
Thus, the diffracted signal contains more energy than the
signal which interacts with the rough ocean, for the 35 knot
wind condition.

In spite of the difficulties with the variable source,
there was one portion of the frequency domain analysis which
was apparently valid. This was because data concerning the
use of either of the seamount models with a model ocean tended
to have the same kinds of variability. Thus when a ratio of
two frequency spectra involving an ocean is formed, the varia-
bility tended to divide out. This is shown in Figure 22.
Here a comparison is made between the 2D and 3D seamount
models with different types of oceans over each. The dashed
line reaches a fairly stable relative value of -3 dB. This
was calculated by subtracting the frequency data obtained for
the 3D model with the average rough ocean from the 2D model
with a smooth ocean. Thus the decibels are relative.

The solid line reaches a fairly stable level of +7 dB.
This was calculated by subtracting the frequency data for the
2D model with the average rough ocean from the 3D model with
the average rough ocean. Here, again, the decibels are rela-
tive. Thus in a pseudo equation approach

dashed line   2D, Smooth Ocean - 3D, Rough Ocean   =   - 3 dB

solid line   <u>3D, Rough Ocean   - 2D, Rough Ocean   =   + 7 dB</u>

                     2D, Smooth Ocean - 2D, Rough Ocean   =   + 4 dB

(40)
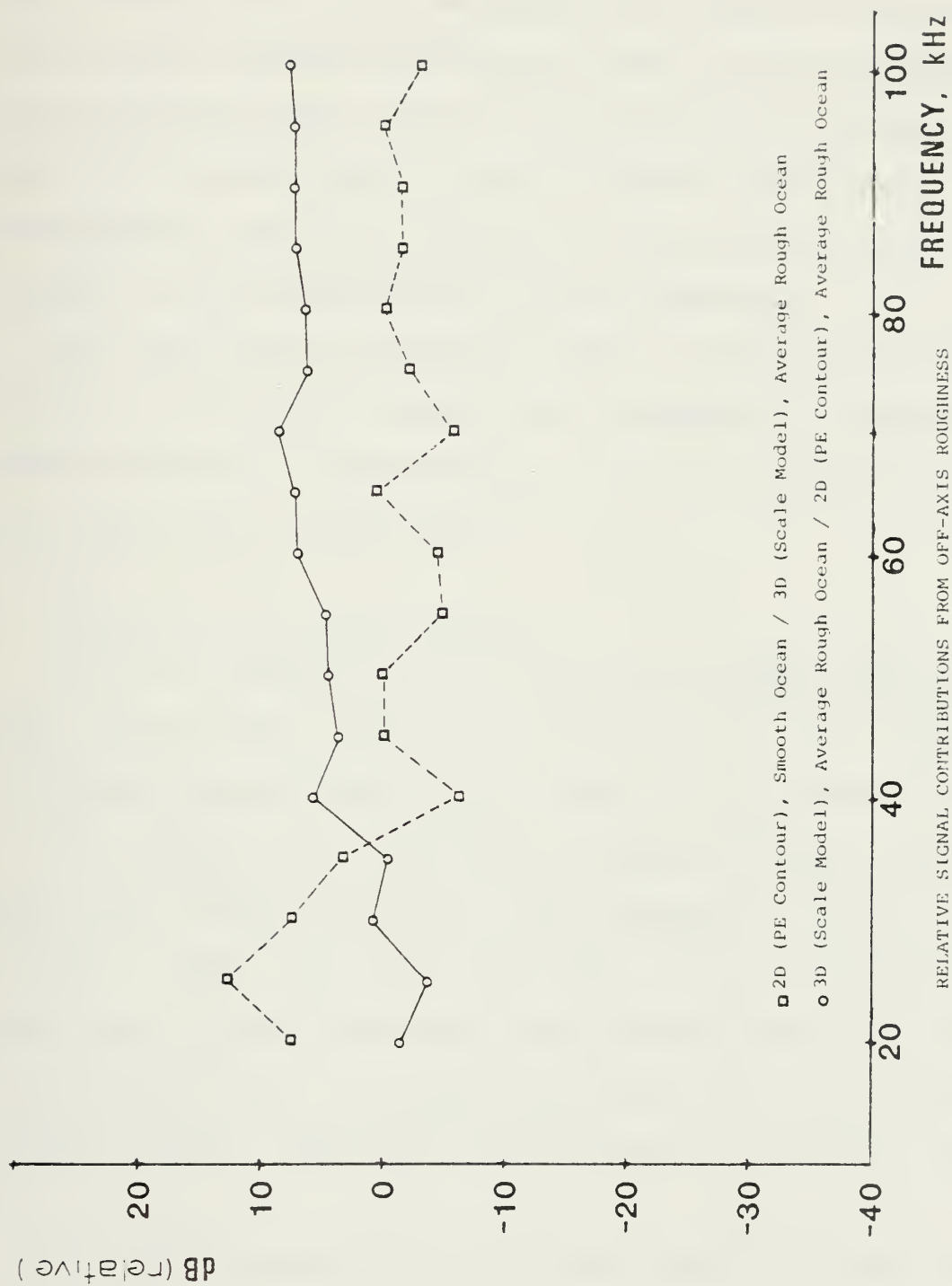
RELATIVE SIGNAL CONTRIBUTIONS FROM OFF-AXIS ROUGHNESS
ELEMENTS AND SCATTERING FROM ROUGH OCEAN

FIGURE 22

□ 2D (PE Contour), Smooth Ocean / 3D (Scale Model), Average Rough Ocean

○ 3D (Scale Model), Average Rough Ocean / 2D (PE Contour), Average Rough Ocean

69

The second equation implies that approximately +7 dB is being contributed by roughness elements on the surface of the 3D model which are off the aixs of transmission. With the 2D model there is no mechanism for acoustic energy that is not being transmitted directly along the acoustic axis to be scattered back into the transmission path; whereas with the 3D model there is, and it seems to be contributing a relatively significant amount of energy to the signal received in the shadow zone, near the seamount.

The third equation suggests that in the far field the presence of the smooth ocean above the seamount increases the received signal by approximately +4 dB when compared to the same model with a rough ocean.

B. RANDOMLY ROUGH PLANE SURFACE

After the rough plate data and the reference data had been collected and recorded on magnetic disk, the boundary wave amplitude and phase and the ratio of the boundary wave to the reference wave amplitude and phase were calculated for each angle and each range for the frequencies 2.5 kHz, 5 kHz, 7.5 kHz, 10 kHz, 12.5 kHz, and 15 kHz. Then all angles for each range and each frequency were averaged using N-1 weighting to give a mean and standard deviation for each frequency and each range. These data are contained in Table IV, Appendix B.

With this processed data available there were four essential comparisons that needed to be made with Tolstoy's theory

70

for hemispherical scattering elements in an effort to establish if the theory could be extended to the case of random roughness. The first was to determine the meaning of $kh \leq 1$ when this was reevaluated using the spatial correlation length, L, of the gravel instead of the center to center spacing, h, of the hemispherical bosses. The second was to investigate the power law governing the amplitude ratio as a function of frequency.

The third was to investigate the power law governing the amplitude ratio as a function of range. The fourth was to attempt an empirical determination of the scattering parameter, ε, of the randomly rough surface by comparing the data with the scattering parameter calculated for the hemispherical bosses.

In the work done by Bailie [Ref. 37], Medwin et al., [Ref. 38], and Hollis [Ref. 39] using the hemispherical bosses, the scattering parameter was $\varepsilon = \sigma h = 8.88 \times 10^{-5}$ m where h is the center to center spacing of the bosses.

To extend this to the case of random roughness, the correlation length, L, was substituted for h. Therefore

$$kL \leq 1 \tag{41}$$

As can be seen in Figures 23 through 26, a sharp peak is reached at 10 kHz. If it is assumed that this frequency marks the limit of coherence

71

$$\frac{2\pi}{C} \text{ (10 kHz) L } = 1$$

$$= \frac{345}{(2\pi)(10 \text{ kHz})} \tag{42}$$

$$= 5.5 \text{ mm}$$

This is in good agreement with the measured correlation length of the gravel surface of

$$L = 4.8 \text{ mm} \tag{43}$$

Thus, the use of the spatial correlation length as defining the limit of coherent scatter in extending Tolstoy's boundary wave theory is appropriate.

The next question addressed was the power law of the amplitude ratio as a function of frequency. The values of the amplitude ratio versus frequency on a log-log scale are contained in Figures 23 through 26. Using linear regression techniques, the slope of the best straight line fit from 2.5 kHz to 10 kHz was calculated for each of the four ranges. The average slope for the amplitude ratio as a function of frequency was then calculated from these four slopes using N-1 weighting. That average slope was +1.50 which is in agreement with the predicted slope of 3/2.

The third question addressed was the power law associated with the amplitude ratio as a function of range. Figures 27 through 30 are the plots of amplitude ratio versus range on a log-log scale for each frequency from 2.5 kHz to 10 kHz.

RATIO OF BOUNDRY WAVE AMPLITUDE TO
VOLUME WAVE AMPLITUDE AS A FUNCTION
OF FREQUENCY. THEORY LINE USING THE
SCATTERING PARAMETER FOR HEMISPHERICAL
BOSSES h = 0.2 CM

FIGURE 23

73

RATIO OF BOUNDRY WAVE AMPLITUDE TO
VOLUME WAVE AMPLITUDE AS A FUNCTION
OF FREQUENCY. THEORY LINE USING THE
SCATTERING PARAMETER FOR HEMISPHERICAL
BOSSES h = 0.2 CM

FIGURE 24

74

RATIO OF BOUNDRY WAVE AMPLITUDE TO
VOLUME WAVE AMPLITUDE AS A FUNCTION
OF FREQUENCY.   THEORY LINE USING THE
SCATTERING PARAMETER FOR HEMISPHERICAL
BOSSES h = 0.2 CM

FIGURE 25

75

RATIO OF BOUNDRY WAVE AMPLITUDE TO
VOLUME WAVE AMPLITUDE AS A FUNCTION
OF FREQUENCY. THEORY LINE USING THE
SCATTERING PARAMETER FOR HEMISPHERICAL
BOSSES h = 0.2 CM

FIGURE 26

76

RATIO OF BOUNDRY WAVE AMPLITUDE TO
VOLUME WAVE AMPLITUDE AS A FUNCTION
OF RANGE. THEORY LINE USING SCATTERING
PARAMETER FOR HEMISPHERICAL BOSSES h = 0.2 CM

FIGURE 27

RATIO OF BOUNDRY WAVE AMPLITUDE TO
VOLUME WAVE AMPLITUDE AS A FUNCTION
OF RANGE.   THEORY LINE USING SCATTERING
PARAMETER FOR HEMISPHERICAL BOSSES h = 0.2 CM

FIGURE 28

RATIO OF BOUNDRY WAVE AMPLITUDE TO
VOLUME WAVE AMPLITUDE AS A FUNCTION
OF RANGE.   THEORY LINE USING SCATTERING
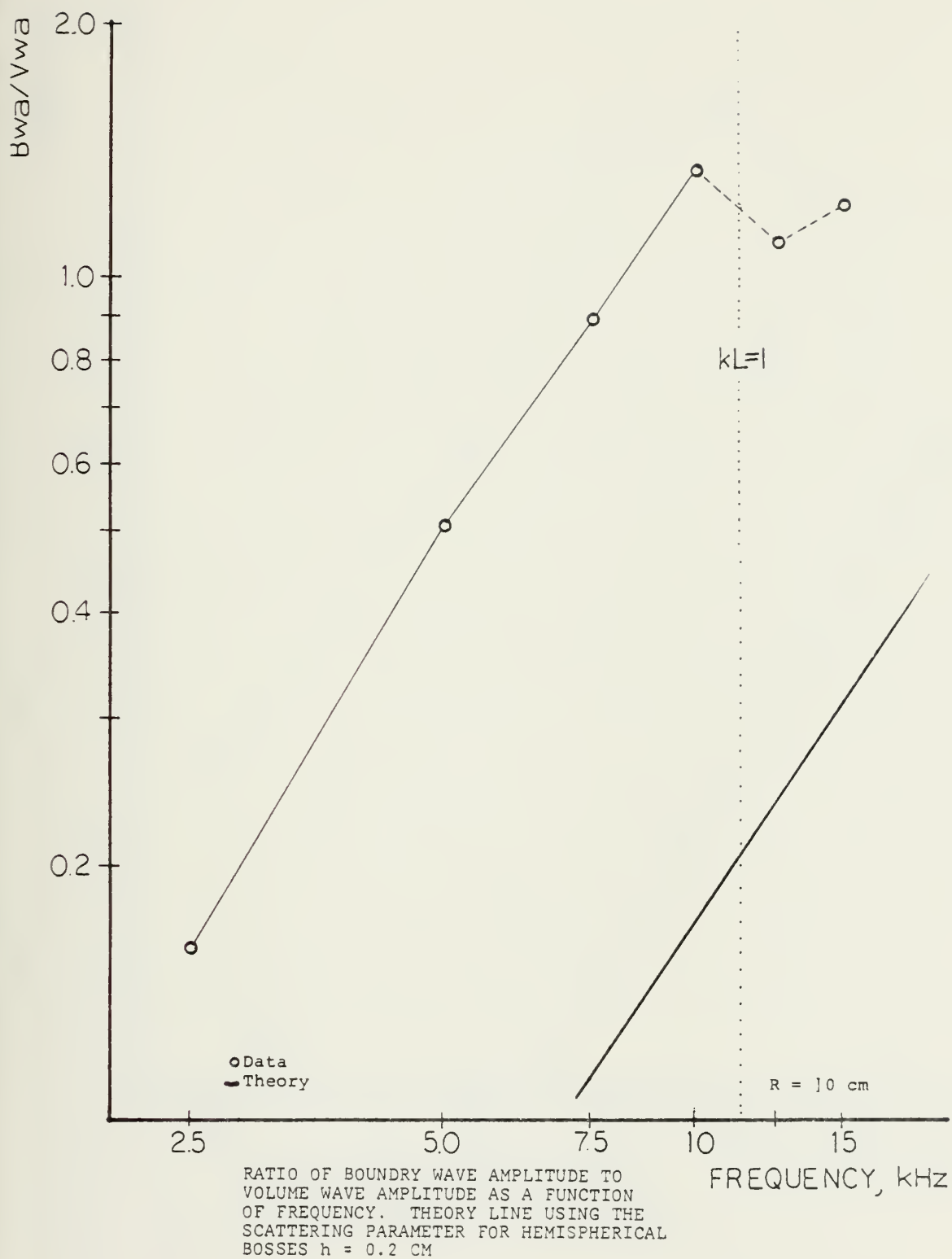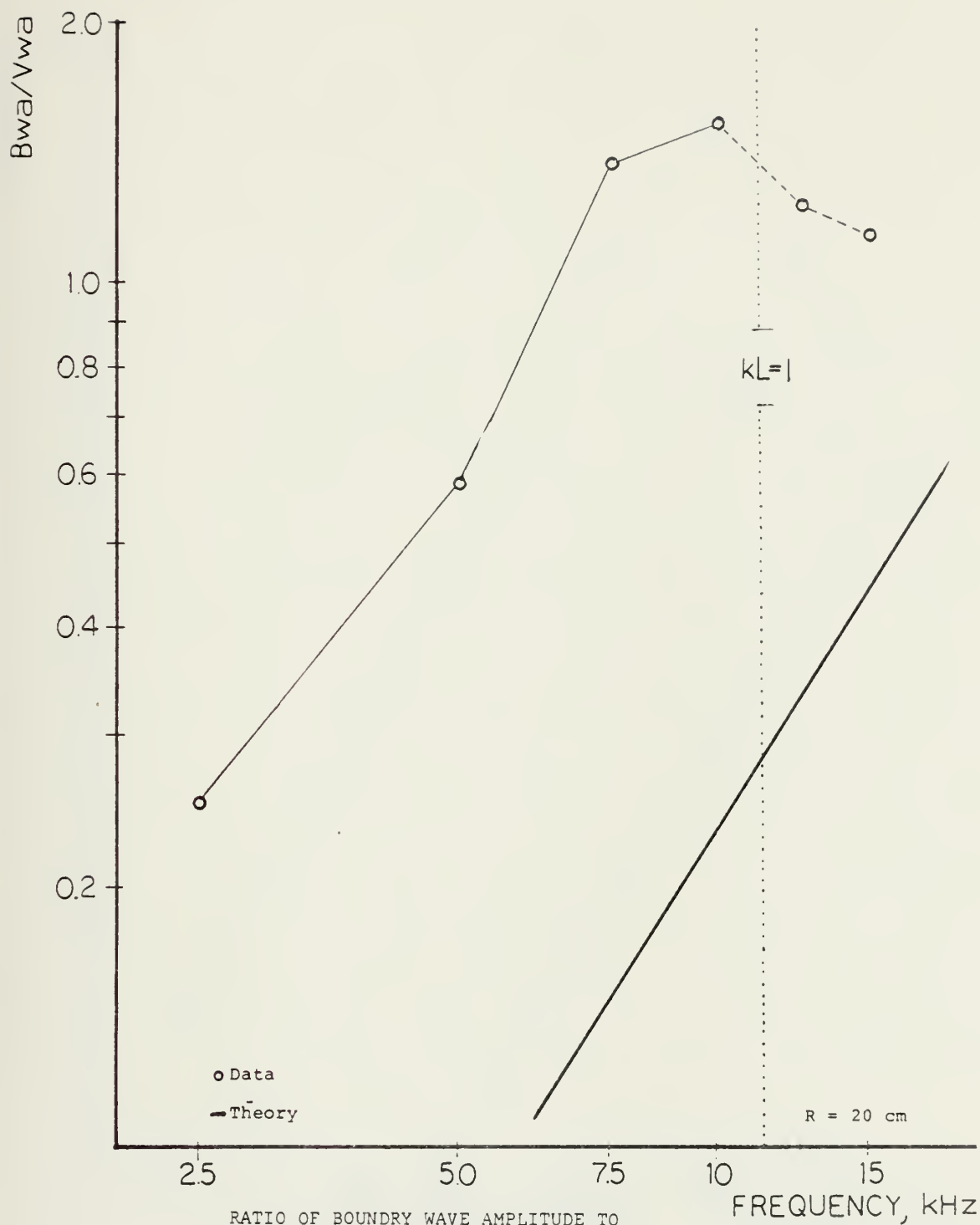PARAMETER FOR HEMISPHERICAL BOSSES h = 0.2 CM

FIGURE 29

79

RATIO OF BOUNDRY WAVE AMPLITUDE TO
VOLUME WAVE AMPLITUDE AS A FUNCTION
OF RANGE. THEORY LINE USING SCATTERING
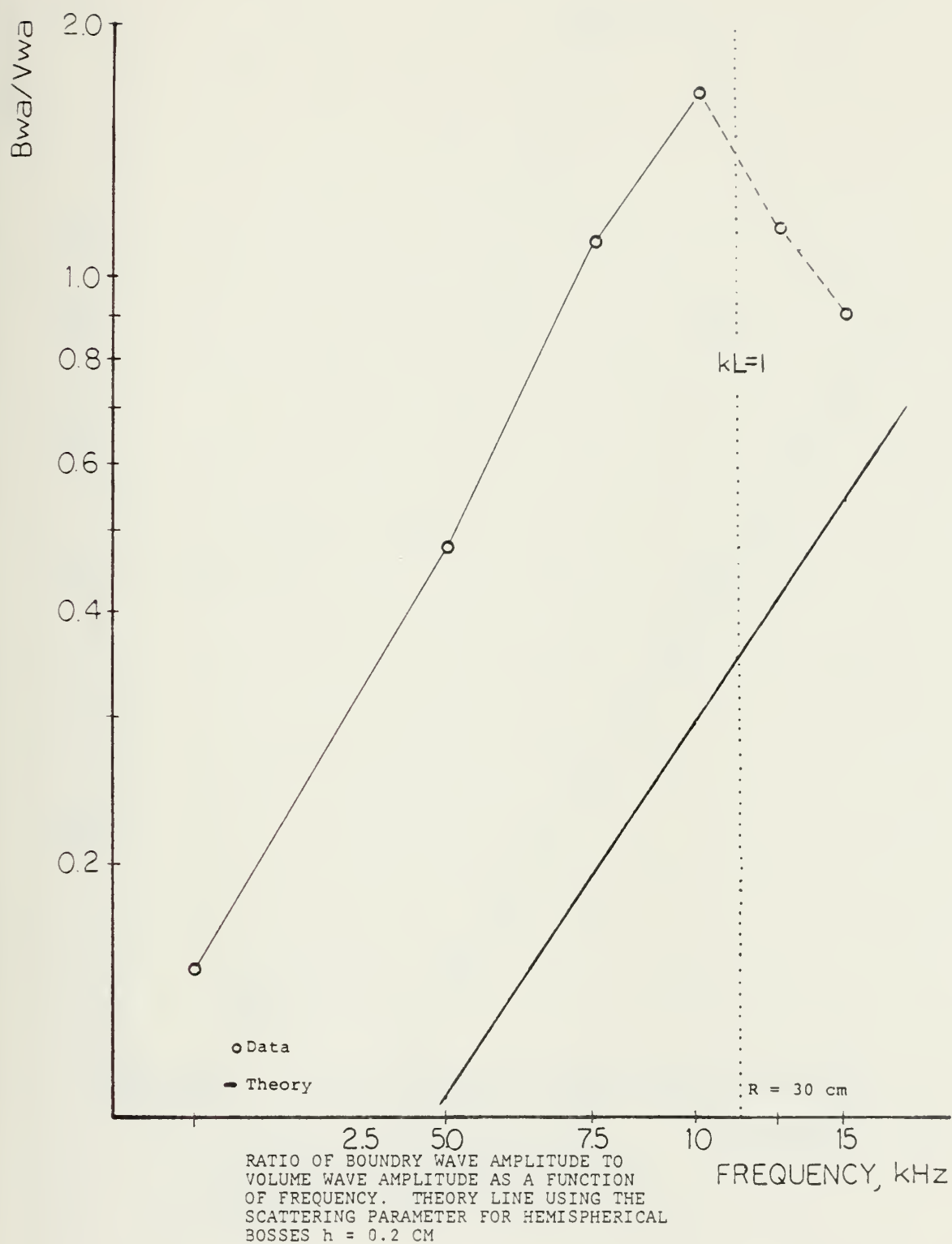PARAMETER FOR HEMISPHERICAL BOSSES h = 0.2 CM

FIGURE 30

80

As can be seen from these figures, there is no clear agreement with theory in this case; although the average of the four slopes is +0.43. Since the agreement was so striking between theory and data for the case of amplitude ratio as a function of frequency, this cannot be discounted. More experimentation would be necessary before anything definitive could be said about the range dependence.

Finally the question of an empirically derived scattering parameter was addressed. It was assumed that the average data as listed in Table III, Appendix B was the value of Tolstoy's theory for a particular range, frequency, and unknown scattering parameter

$$[\frac{BWA}{VWA}] \ = \ \varepsilon_R \ (2\pi r)^{1/2} \ k^{3/2} \tag{44}$$

where

$$r \ = \ \text{a specified range}$$

$$k \ = \ \text{wave number at a specified frequency}$$

$$\varepsilon_R \ = \ \text{unknown scattering parameter}$$

Then, if Equation (24) were evaluated at that same range and frequency then divided into the data value in question,

$$\frac{\text{Data Value}}{\text{Calculated Value}} \ = \ \frac{\varepsilon_R (2\pi r)^{1/2} \ k^{3/2}}{\varepsilon_T (2\pi r)^{1/2} \ k^{3/2}} \tag{45}$$

$$= \ \frac{\varepsilon_R}{\varepsilon_T}$$

81

where

$$\varepsilon_T = 8.88 \times 10^{-5} \text{ m}$$

as calculated for the case of hemispherical bosses with 0.2 cm center to center spacing. The resultant number is then multiplied by the theoretical scattering parameter for the hemispherical bosses

$$\frac{\text{Data Value}}{\text{Calculated Value}} \times \varepsilon_T = \varepsilon_R \qquad (46)$$

This procedure was followed and a numerical value for the scattering parameter was found for each range and frequency. The resultant 16 numbers were averaged using N-1 weighting. As reported in Ref. 16, the scattering parameter for the hemispherical bosses was

$$\varepsilon = 0.300 \, \sigma \qquad (47)$$

where σ was the rms height of the hemispherical bosses. Following this approach using the calculated statistics for the gravel

$$\bar{\varepsilon}_R = n \, \sigma \qquad (48)$$

where

$\bar{\varepsilon}_R$ = average scattering parameter for gravel = 6.03×10^{-4} m

n = numerical coefficient which was 0.300 for the case of hemispherical bosses

then

$$n = \frac{\overline{\varepsilon}_R}{\sigma} = 0.27 \qquad (49)$$

This result implies that the scattering parameter as pre-dicted by Tolstoy for hemispherical bosses is the same for the randomly rough plane surface.

VI. CONCLUSIONS

A. SEAMOUNT

If the pressure versus time graphs in Figure 25 are com-
pared, the first pulse observed in the 79 km shadowing sit-
uation at sea [Ref. 40] was the direct diffracted signal and
the second pulse was the surface scattered energy. The time
separation observed in the laboratory between these two
groups of energy correspond to that which Chapman [Ref. 41]
and Ebbeson observed at sea. This concept is represented
graphically in Figure 31. In this figure the time from the
onset of the signal until 203 microseconds is from the graph
of the energy diffracted over the 3D seamount model; while
the time from 203 microseconds until 603 microseconds is
from the graph of the 3D seamount model with a rough ocean.
Second, if the entire graph of pressure versus time for the
seamount with a smooth ocean is compared with that of the
seamount with a rough ocean (the bottom two graphs of Figure
24), the distinctly different nature of a reflection dominated
situation and a diffraction dominated situation becomes more
apparent. When the ocean is smooth, multiple reflections are
the principal source of energy. When the ocean is roughened
by a 35 knot wind the diffracted pulse (the first pulse) is
stronger than the multi-scattered, surface-to-seamount,
energy (second and later pulses). A CW experiment would be
diffraction dominated with these seas.

FIGURE 31.   Composite pressure versus time showing diffraction
only first pulse and scattered second and later pulses

85

B. RANDOMLY ROUGH PLANE SURFACE

The work done with the randomly rough plane surface constitutes a first look at the problem of extending Tolstoy's boundary wave theory to the real world. The work done in this thesis suggests that Tolstoy's theory can be applied to the real problem of a randomly rough rigid surface. This is of fundamental importance because of the decreased loss by geometric spreading that the boundary wave suffers relative to smooth surface spreading.

To this point the seamount and the randomly rough plane surface have been discussed as if they were separate problems. In reality they are not. The Dickens Seamount in the Gulf of Alaska has small scale roughness on its surface which has not been represented on the 3D model. Because of the great depths of Dickens Seamount this small scale roughness has never been observed. However, as stated by Chapman [Ref. 42] the spectra for the shot data collected at sea show a curious interference pattern at a relatively stable frequency difference whenever ray diagrams indicate the acoustic wave is interacting with the seamount. As pointed out by Hollis [Ref. 43] for the case of a 14 degree wedge and hemispherical bosses, there was a pronounced boundary wave diffracted over the crest of the wedge in his experiments. The phase speed for the boundary wave is slightly less than that of the volume wave [Refs. 44, 45]. It has been suggested by Medwin [Ref. 46] that the presence of the interference pattern in the

frequency data from DREP is evidence that the effects of the boundary wave may have already been observed in nature.

APPENDIX A

TABLE II

EQUIPMENT SETTINGS FOR SEAMOUNT EXPERIMENT

A. Timing Simulator

Word	Output	Time
0	1	100 μsec
1	0	4 msec
2	0	10 μsec
3	3	900 μsec
4	0	20 msec

B. ARB

1) Mode = trig

2) block rate = 1 kHz

3) func = RAM 8

X	Y
0	127
1	-127
0-255	0

4) amp = 0.5 V

C. Polarization Voltage = +150 VDC

D. Power Amplifier

Ω	A	V
108	2.5	265

E. PARS

1) Gain = 100

2) Gain = 20

F. BP Filter

1) Pass Band = 6 kHz - 40 kHz

2) Pass Band = 20 Hz - 200 kHz

TABLE III

EQUIPMENT SETTINGS FOR RANDOMLY ROUGH PLANE SURFACE EXPERIMENT

A. ARB

    1) mode = trig

    2) block rate = 2.5 kHz

    3) func = tri

    4) starting addr = 126

    5) amp = 0.35 V

B. Polarization Voltage = +150 VDC

C. Power Amplifier = 220 V

D. BP Filter

    1) Pass Band = 500 Hz to 110 kHz

    2) Pass Band = 500 Hz to 110 kHz

E. Range Dependent Settings:

    R = 40 cm

Timing Simulator			PARS	
word	output	time	1	2
0	1	100 μsec		
1	0	1 msec	50	100
2	0	400 μsec		
3	3	5 msec		
4	0	25 msec		

    R = 30 cm

word	output	time	1	2
0	1	100 μsec		
1	0	1 msec	50	100
2	0	120 μsec		
3	3	5 msec		
4	0	25 msec		

R = 20 cm

0	1	100 µsec		
1	0	800 µsec	20	100
2	3	5 msec		
3	0	25 msec		

R = 10 cm

0	1	100 µsec		
1	0	510 µsec	20	100
2	3	5 msec		
3	0	25 msec		

APPENDIX B

TABLE IV

AVERAGE AMPLITUDE DATA BY RANGE AND FREQUENCY

	Freq (kHz)	BWA (average)	BWA/VWA (average)
R = 40 cm	2.5	13.76	0.41
	5	11.04	0.45
	7.5	52.25	1.84
	10	35.86	1.94
	12.5	38.40	1.23
	15	16.88	0.91
R = 30 cm	2.5	5.12	0.15
	5	13.81	0.48
	7.5	36.17	1.12
	10	40.18	1.69
	12.5	43.92	1.17
	15	23.56	0.92
R = 20 cm	2.5	5.01	0.25
	5	10.58	0.59
	7.5	27.74	1.39
	10	33.98	1.56
	12.5	32.06	1.25
	15	17.77	1.16
R = 10 cm	2.5	6.36	0.16
	5	17.98	0.51
	7.5	36.20	0.90
	10	60.14	1.36
	12.5	59.46	1.12
	15	39.88	1.24

LIST OF REFERENCES

1. Biot, M.A. and Tolstoy, I., "Formulation of Wave Propagation In Infinite Media by Normal Coordinates with an Application to Diffraction," The Journal of The Acoustical Society of America, V. 29, p. 381-391, 1957.

2. Bremhorst, J.H., "Impulse Wave Diffraction by Rigid Wedges and Plates," M.S. Thesis, U.S. Naval Postgraduate School, Monterey, CA, 1978.

3. Spaulding, J.P. Jr., "Physical Modeling of Sound Shadowing by Seamounts," M.S. Thesis, U.S. Naval Postgraduate School, Monterey, CA, 1979.

4. Ebbeson, G.R., Thorleifson, J.M. and Turner, R.G., "Shadowing of Sound Propagation by a Seamount in the North Pacific," The Journal of the Acoustical Society of America, V. 64, S(76), 1978.

5. Medwin, H., and Spaulding, R.P., "The Seamount as a Diffracting Body," pp. 421-428 in "Bottome Interacting Ocean Acoustics," ed. W.A. Kuperman and F.B. Jensen, Plenum Press, New York, 1980. 11 June 1980.

6. Tolstoy, I., "The Scattering of Spherical Pulses by Slightly Rough Surfaces," The Journal of the Acoustical Society of America, V. 66, p. 1135-1144, 1979.

7. Biot, M.A., "Generalized Boundary Condition for Multiple Scatter in Acoustical Reflection," The Journal of the Acoustical Society of America, V. 44, p. 1616-1622, 1968.

8. Bailie, J.M., "Near Grazing Scattering by Slightly Rough Surfaces," M.S. Thesis, U.S. Naval Postgraduate School, Monterey, Ca, 1978.

9. Hollis, S.J., "The Propagation of a Scattered Acoustic Boundary Wave Over a Rough Wedge," M.S. Thesis, U.S. Naval Postgraduate School, Monterey, CA, 1980.

10. Spaulding, J.P. Jr., "Physical Modeling of Sound Shadowing by Seamount," M.S. Thesis, U.S. Naval Postgraduate School, Monterey, CA, 1979.

11. Medwin, H., "Shadowing by Finite Noise Barriers," April 1981.

12. Biot, M.A., "Generalized Boundary Condition for Multiple Scatter in Acoustical Reflection," The Journal of the Acoustical Society of America, V. 44, p. 1616-1622, 1968.
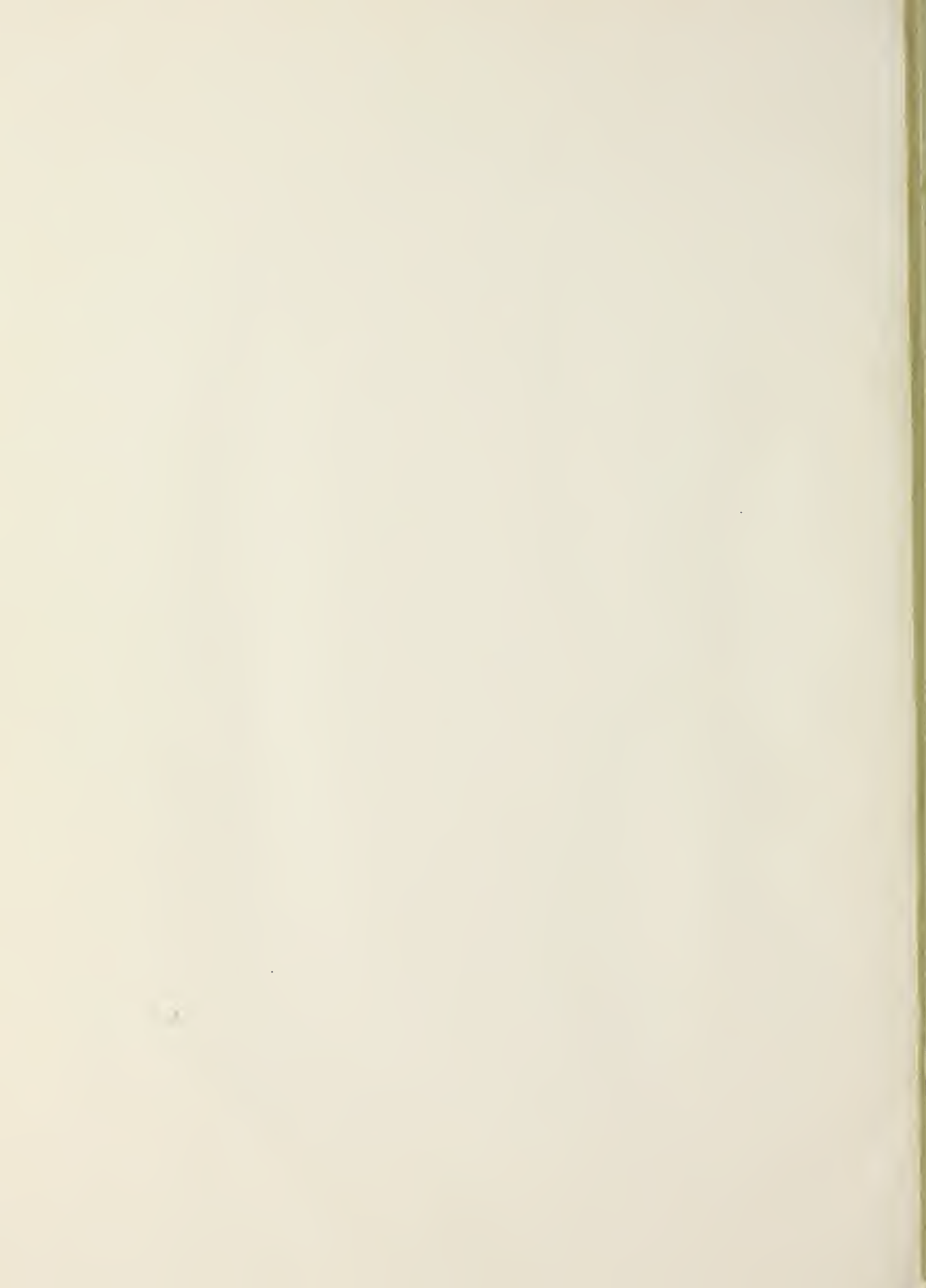
13.   Ibid., pp. 1616-1622.

14.   Ibid., pp. 1616-1622.

15.   Bailie, Op. Cit.

16.   Medwin, H., Bailie, J.M., Bremhorst, J.H., Savage, B.J.,
      and Tolstoy, I., "The Scattered Acoustic Boundary Wave
      Generated by Grazing Incidence at a Slightly Rough Rigid
      Surface," The Journal of the Acoustical Society of
      America, V. 66, p. 1131-1134, 1979.

17.   Hollis, Op. Cit.

18.   Ibid.

19.   Spaulding, J.P. Jr., "Physical Modeling of Sound Shadow-
      ing by Seamounts," M.S. Thesis, U.S. Naval Postgraduate
      School, Monterey, Ca, 1979.

20.   Ibid.

21.   Ebbeson, et al., Op. Cit.

22.   Jensen, F.B., Kuperman, W.A. and Medwin, H., "Propagation
      Over a Seamoutn," paper presented at 100th Meeting of
      the Acoustical Society of America, Los Angeles, Ca,
      19 November 1980.

23.   Spaulding, J.P. Jr., "Physical Modeling of Sound Shadow-
      ing by Seamounts," M.S. Thesis, U.S. Naval Postgraduate
      School, Monterey, Ca, 1980.

24.   Hollis, Op. Cit.

25.   Medwin, H., "The Rough Surface and Bubble Effects on Sound
      Propagation in a Surface Duct," NPS - 61Md 71101A, U.S.
      Naval Postgraduate School, Monterey, Ca 1971.

26.   Spaulding, J.P. Jr., "Physical Modeling of Sound Shadow-
      ing by a Seamount," M.S. Thesis, U.S. Naval Postgraduate
      School, Monterey, Ca, 1979.

27.   Ebbeson, et al., Op. Cit.

28.   Jordan, E.A. and Medwin, H., "Scale Model Studies of
      Scattering and Diffraction at a Seamount," paper pre-
      sented at the 101st Meeting of the Acoustical Society of
      America, Ottawa, Canada, 20 May 1981.

29.   Spaulding, J.P., Jr., "Physical Modeling of Sound Shadow-
      ing by a Seamount," M.S. Thesis, U.S. Naval Postgraduate
      School, Monterey, Ca, 1979.

30. Bailie, Op. Cit.

31. Hollis, Op. Cit.

32. Frederiksen, E., "Condenser Microphones Used as Sound Sources," Bruel and Kjaer Technical Review, No. 3, 1977.

33. Stark, H. and Tuteur, F.B., Modern Electrical Communications Theory and Systems, p. 139-141, Prentice-Hall, Inc., 1979.

34. Bailie, Op. Cit.

35. Hollis, Op. Cit.

36. Ebbeson, et al., Op. Cit.

37. Bailie, Op. Cit.

38. Medwin, Bailie, Bremhorst, Savage and Tolstoy, Op. Cit.

39. Hollis, Op. Cit.

40. Chapman, N.R. and Ebbeson, G.R., "Multi-path Propagation Loss Measurements over an Isolated Seamount," paper presented at the 101st Meeting of the Acoustical Society of America, Ottawa, Canada, 20 May 1981.

41. Ibid.

42. Chapman, N.R., personal communication.

43. Hollis, Op. Cit.

44. Ibid.

45. Medwin, H., paper in preparation.

46. Medwin, H., personal communication.

INITIAL DISTRIBUTION LIST

No. Copies

1. Defense Technical Information Center   2
    Cameron Station
    Alexandria, Virginia 22314

2. Library, Code 0142   2
    Naval Postgraduate School
    Monterey, California 93940

3. Department Chairman, Code 61   1
    Department of Physics and Chemistry
    Naval Postgraduate School
    Monterey, California 93940

4. Professor H. Medwin, Code 61Md   6
    Department of Physics and Chemistry
    Naval Postgraduate School
    Monterey, California 93940

5. Manager, Anti-Submarine Warfare Systems   1
    Project Office (ASW 13)
    Attn: CDR. J. Hagy
    Department of the Navy
    Washington, D.C. 20362

6. Office of Naval Reserach
    Arlington, Virginia 22217
    Attn: CODE 480   3
    Attn: CODE 486   1
    Attn: CODE 460   1
    Attn: CODE 102-05   1

7. Dr. I. Tolstoy   1
    Knockvennie
    Castle Douglas, KIRKS
    Scotland, United Kingdom

8. Defense Research Establishment, Pacific
    F.M.O. Victoria, British Columbia, VOS 1 60
    Canada
    Attn: Mr. G.R. Ebbeson   1
          Dr. N. Ross Chapman   1

9. LCDR. J.M. Bailie, USN   1
    504 Pondview Circle
    Virginia Beach, Virginia 23452

10. Lt. S.P. Spaulding, USN   1
    11 Wisk-Key Wind Road
    Wallingford, Connecticut 06492

11. Lt. S.J. Hollis, USN   1
    1218 East Walnut
    Springfield, Missouri 65802

12. Lt. E.A. Jordan, USN   2
    312 Maple W. P.O. Box 179
    Hansen, Idaho 83334

13. Naval Electronics System Command   6
    Code 612 (Attn: Lt. Hollis)
    Washington, D.C. 20360